Appl. Comput. Harmon. Anal. 31 (2011) 325–345

Contents lists available at ScienceDirect

Applied and Computational Harmonic Analysis

www.elsevier.com/locate/acha

Inversion of the noisy Radon transform on $SO(3)$ by Gabor frames and sparse recovery principles

Paula Cerejeiras [a], Milton Ferreira [b], Uwe Kähler [a], Gerd Teschke [c,*]

[a] Center of Research and Development in Mathematics and Applications, University of Aveiro, Department of Mathematics, 3810-193 Aveiro, Portugal
[b] ESTG – Polytechnical Institute of Leiria, Department of Mathematics, 2411-901 Leiria, Portugal
[c] Neubrandenburg University of Applied Sciences, Institute for Computational Mathematics in Science and Technology, Brodaer Str. 2, 17033 Neubrandenburg, Germany

ARTICLE INFO

Article history:
Received 15 January 2010
Revised 23 December 2010
Accepted 12 January 2011
Available online 20 January 2011
Communicated by W.R. Madych

Keywords:
Radon transform on $SO(3)$
X-ray tomography
Gabor frames
Coorbit theory
Sparse recovery
Crystallography

ABSTRACT

The inversion of the one-dimensional Radon transform on the rotation group $SO(3)$ is an ill-posed inverse problem that can be applied to X-ray tomography with polycrystalline materials. This paper is concerned with the development of a method to stably approximate the inverse of the noisy Radon transform on $SO(3)$. The proposed approach is composed by basic building blocks of the coorbit theory on homogeneous spaces, Gabor frame constructions and variational principles for sparse recovery. The performance of the finally obtained iterative approximation is studied through several experiments.

1. Introduction

The Radon transform on $SO(3)$ becomes an instrument in crystallographic texture analysis as it relates the crystallographic orientation density function (ODF) and its experimentally accessible pole density functions (PDFs), see [25,4,22]. The determination of a suitable ODF from pole intensity data can be done through the inversion of the Radon transform on $SO(3)$. Several inversion methods (mostly ad hoc procedures) have been studied in the past, see e.g. [5,15,17,18,24]. To our knowledge an important contribution with mathematical rigor in this field was given by [16] in which a Fourier slice theorem for the Radon transform on $SO(3)$ characterizing the Radon transform as a multiplication operator in Fourier space was elaborated. The authors of [16] present a fast algorithm for the evaluation of the discrete inverse Radon transform in $SO(3)$ based on fast Fourier techniques on the two-dimensional sphere S^2 and the rotational group $SO(3)$.

The procedure presented in this paper is completely different and goes as follows. We consider the Radon transform R as a map between $L_2(S^3)$ and $L_2(S^2 \times S^2)$ (which is in this setting an ill-posed operator). To numerically compute an approximation to the solution of the inverse problem $Rf = g$, we have to establish a suitable and reasonable expansion for f. Assuming sparsely localized orientation density functions (and also hoping to achieve some technical operability), we focus on Gabor system expansions for $L_2(S^3)$. This also allows us to work with a spherical grid (representing the translates of the window function), which is given in terms of the binary icosahedral group (given by the vertices of the 600-cell). Such a distribution seems to us suitably adapted to the study of ODF's which are invariant under a certain point group (hence, subgroup of the orthogonal group) determined by the crystal under study. 14 crystallographic point groups (e.g. the

* Corresponding author.
E-mail address: teschke@zib.de (G. Teschke).

1063-5203/$ – see front matter
doi:10.1016/j.acha.2011.01.005

cyclic groups C_2, and C_3, the dihedral group D_3, and the tetrahedral group T) are (up to a covering) subgroups of the binary icosahedral group. Therefore, it exists at least a large class of ODF's for which it makes sense to assume sparsity of the ODF with the respect to the translation grid of the Gabor frame. In order to establish such a localized Fourier system on S^3, we shall involve the machinery of group representation theory. The construction of associated function spaces and suitable discretizations in them (i.e. the construction of frames) requires a certain concept of function spaces. Here we shall rely on the coorbit theory as it was developed in [8,7]. With these concepts at hand, we then address the problem of computing an approximate solution of the linear inverse problem. Unfortunately, the function g is in many practical situations not exactly given but only a noisy version g^δ of g with $\|g - g^\delta\| \leqslant \delta$ is available. Consequently, due to the ill-posedness of R we are therefore faced with regularization issues. To stabilize the inversion process, we propose an iterative procedure that will emerge from the minimization of a residual based variational formulation of the inversion problem. This variational formulation also involves some sparsity constraints leading to thrifty expansions of the ODF. The minimization procedure is close to techniques that were proposed in [11–13,27] and [9,28].

The organization of the paper is as follows. In Section 2 we establish the analytical framework that seems to be well-suited for the problem of inverting the Radon transform on $SO(3)$. In particular, we define the Gabor transform, its admissibility, corresponding coorbit spaces, atomic decompositions and frames. In Section 3 we focus on the problem of stably approximating the inverse of the Radon transform on $SO(3)$. Due to the curse of dimensionality, we discuss very efficient approximation techniques as well as thrifty strategies for the computation of the stiffness matrix entries. In the end of this section we consider a crystallographic recovery problem (synthetic example). Appendix A contains material on the algebra of quaternions.

2. Preliminaries and analytical framework

Within this section we set up the analytical framework suited for our problem of inverting the Radon transform on $SO(3)$. We start by introducing a group theoretical signal analysis approach, namely the Gabor transform on $SO(3)$, and verify by classical techniques that this transform acts isometrically between $L_2(S^3)$ and $L_2(Spin(4) \times \mathbb{R}^3)$. Due to nice localization properties the Gabor transform is well suited for expanding localized functions on $L_2(S^3)$. In order to construct Gabor systems on $L_2(S^3)$, we briefly review the concept of coorbit theory on homogeneous spaces that was developed in [7,8]. The coorbit theory was primarily designed to describe the much broader concept of Banach spaces on the basis of square integrable group representations. But even the restriction to Hilbert spaces is very helpful for our purposes as it furnishes the underlying function space $L_2(S^3)$ with frames for adequately expanding the functions. Proceeding this way we have ansatz systems at our disposal that allow sparse representations (efficient through localization) of ODF functions that we aim to recover and feasible discretizations of the Radon transform operator.

2.1. Gabor transform on $L_2(SO(3))$

In order to establish Gabor analysis for the Hilbert space $L_2(SO(3))$, we first have to identify a suitable phase space G (as a substitute to the Weyl–Heisenberg group) for the Gabor transform on $L_2(SO(3))$. To relate the Gabor transform image space $L_2(G)$ with $L_2(SO(3))$, we need to construct a unitary representation of G on $L_2(SO(3))$. This group representation should be preferably square integrable, thus ensuring that the associated Gabor transform is an isometry between $L_2(SO(3))$ and $L_2(G)$.

Let us first find a suitable characterization of $SO(3)$. There are many coordinate systems and set of parameters for describing the group of rotations in $\mathbb{R}^3$. The coordinate system is typically chosen depending on the underlying application. For our purpose, we consider instead of $SO(3)$ its double covering group $Spin(3)$, which is diffeomorphic to the symplectic group $Sp(1)$ of the unit quaternions (3-sphere). For details we refer to Appendix A.2. With this description, we can follow the ideas of Torrésani, see [29], and construct a version of the windowed Fourier transform on the sphere. Since the usual Fourier transform is generated by translations and modulations, we need similar transformations on the sphere. A natural candidate is the Euclidean group $G := E(4) = Spin(4) \times \mathbb{R}^4$. The group operation in G reads as

$$(s_1, p_1) \circ (s_2, p_2) = (s_1 s_2, p_1 + s_1 p_2 \overline{s_1}) \tag{1}$$

and the inverse element of (s_1, p_1) is

$$(s_1, p_1)^{-1} = (\overline{s_1}, -\overline{s_1} p_1 s_1), \tag{2}$$

where $\overline{s_1}$ denotes the conjugate element of $s_1 \in Spin(4)$ (see [14]). As a natural analogue to the Schrödinger representation of the Weyl–Heisenberg group on $L_2(\mathbb{R}^n)$, we can define the representation of G on $L^2(S^3)$:

$$U(s, p) f(q) := e^{i\langle p, q\rangle} f(\bar{s} q s)$$

with $q \in S^3$. Recall that a unitary representation of a locally compact group G on a Hilbert space is a homomorphism U from G into the group of unitary operators $\mathcal{U}(L_2(S^3))$ on $L_2(S^3)$ which is continuous with respect to the strong operator topology. It is easy to check that U is a homomorphism. Indeed,

$$\begin{aligned} U(s_1,p_1)\big[U(s_2,p_2)f(q)\big] &= U(s_1,p_1)\big[e^{i\langle p_2,q\rangle} f(\overline{s_2}qs_2)\big] \\ &= e^{i\langle p_1,q\rangle} e^{i\langle p_2,\overline{s_1}qs_1\rangle} f(\overline{s_2}\,\overline{s_1}qs_1s_2) \\ &= e^{i\langle p_1+s_1p_2\overline{s_1},q\rangle} f(\overline{s_1s_2}qs_1s_2) \\ &= U\big((s_1,p_1)\circ(s_2,p_2)\big)f(q). \end{aligned}$$

We remark that U is the representation of $E(4)$ induced from the one-dimensional representation ψ of its subgroup $Spin(3)\times\mathbb{R}^4$ given by $\psi(s,x)=e^{i\langle\omega_0,x\rangle}$ where $\omega_0\in S^3$ is a vector fixed by $Spin(3)$. In particular, the Mackay machinery implies that U is irreducible.

As already mentioned in [29], this representation is not square-integrable. To overcome this integrability problem we have to consider U restricted to a suitably chosen section of a quotient group G/H. One natural candidate for H is given by the stability group $H=\{(1,(0,0,0,p_4))\in G:\ p_4\in\mathbb{R}\}$ of G (cf. [29] for details). The following constructions substantially depend on the choice of the section σ of the principal bundle $\Pi: G\to G/H$. We choose the flat section $\sigma(s,p)$ with $p=(\underline{p},0)$, where $\underline{p}=(p_1,p_2,p_3)\in\mathbb{R}^3$, which is sufficient for our purpose. Indeed, since each right coset in G/H is given by varying the last component of p we can find a unique representative by choosing $p_4=0$. The flat section σ just corresponds to this representative.

Then, $X=G/H$ carries the G-invariant measure $d\mu(x)=d\mu(s_x)\,dp_x$, where $\sigma(x)=(s_x,p_x)$. In our case dp_x is just the Lebesgue measure on $\mathbb{R}^3$ and $d\mu(s_x)$ is a spin-invariant measure on $Spin(4)$. It remains to verify that U is indeed strictly square integrable modulo (U,σ). Therefore, we have to prove that there exists a window functions $\psi\in L_1(S^3)$ such that

$$\begin{aligned} V_\psi f(s,p) &= \big\langle f, U\big(\sigma(s,p)^{-1}\big)\psi\big\rangle \qquad (3)\\ &= \int_{S^3} \overline{e^{-i\langle\bar{s}ps,q\rangle}}\,\overline{\psi}(sq\bar{s})f(q)\,dS_q \\ &= \int_{S^3} e^{i\langle p,sq\bar{s}\rangle}\,\overline{\psi}(sq\bar{s})f(q)\,dS_q, \qquad (4) \end{aligned}$$

where dS_x denotes the usual Lebesgue measure on S^3, is an isometry. This we will show by applying techniques of [8,29].

Lemma 1 *(Admissibility and isometry). Assume that the window $\psi\in L_2(S^3)$ is such that $supp(\psi)\subseteq S^3_+=\{q\in\mathbb{H}:\ \|q\|=1\wedge q_0>0\}$, where q_0 denotes the real part of the unit quaternion q (see Appendix* A.1*). Furthermore, we assume it satisfies the admissibility condition*

$$0\neq C_\psi = 64\pi^5\int_0^{2\pi}\int_0^{\pi}\int_0^{\pi/2}\frac{|\psi(q(\theta,\alpha,\phi))|^2}{\cos\phi}\,d\phi\,d\alpha\,d\theta<\infty. \qquad (5)$$

Then the map

$$f\in L^2\big(S^3\big)\mapsto\frac{1}{\sqrt{C_\psi}}V_\psi f\in L^2\big(Spin(4)\times\mathbb{R}^3\big)$$

is an isometry, i.e.

$$\int_{Spin(4)\times\mathbb{R}^3}\big|V_\psi f(s,p)\big|^2\,d\mu(s)\,dp = C_\psi\int_{S^3}\big|f(q)\big|^2\,dS_q.$$

Proof. By a simple substitution we obtain

$$\begin{aligned} \|V_\psi f\|^2 &= \int_{Spin(4)}\int_{\mathbb{R}^3}\left|\int_{S^3} e^{i\langle p,sq\bar{s}\rangle}\,\overline{\psi}(sq\bar{s})f(q)\,dS_q\right|^2 dp\,d\mu(s) \\ &= \int_{Spin(4)}\int_{\mathbb{R}^3}\left|\int_{S^3} e^{i\langle p,q\rangle}\,\overline{\psi}(q)f(\bar{s}qs)\,dS_q\right|^2 dp\,d\mu(s). \end{aligned}$$

Let $q=\Lambda(\theta,\alpha,\phi)$, $\theta\in[0,2\pi[$, $\alpha\in[0,\pi[$ and $\phi\in[0,\pi[$, where Λ denotes the map from spherical to Cartesian coordinates defined by

$$\Lambda(\theta,\alpha,\phi)=\begin{cases} q_0=\cos\phi,\\ q_1=\cos\alpha\sin\phi,\\ q_2=\sin\theta\sin\alpha\sin\phi,\\ q_3=\cos\theta\sin\alpha\sin\phi. \end{cases} \tag{6}$$

Let also $v: S^3_+ \to B^3$ denote the projection map from the upper hemisphere S^3_+ onto the unit ball B^3 (in $\mathbb{R}^3$) obtained by the change of variable $t=\sin\phi$ in (6) and cutting the real component q_0. Consequently,

$$\begin{aligned}\int_{S^3} e^{i\langle p,q\rangle}\overline{\psi}(q)f(\bar{s}qs)\,dS_q &= \int_{B^3} e^{i\langle x(t,\theta,\alpha),\underline{p}\rangle}\overline{\psi}\big(v^{-1}\big(x(t,\theta,\alpha)\big)\big)f\big(\bar{s}v^{-1}\big(x(t,\theta,\alpha)\big)s\big)\frac{t^2\sin\alpha}{\sqrt{1-t^2}}\,dt\,d\theta\,d\alpha\\ &= \mathcal{F}\bigg(\frac{\overline{\psi}(v^{-1}(\cdot))}{\sqrt{1-t^2}}f\big(\bar{s}v^{-1}(\cdot)s\big)\bigg)(\underline{p}),\end{aligned}$$

where $\underline{p}=(p_1,p_2,p_3)$, and $\mathcal{F}$ denotes the Fourier transform on $\mathbb{R}^3$. Applying Plancherel's theorem yields

$$\bigg\|\mathcal{F}\bigg(\frac{\overline{\psi}(v^{-1}(\cdot))}{\sqrt{1-t^2}}f\big(\bar{s}v^{-1}(\cdot)s\big)\bigg)\bigg\|^2_{L^2(\mathbb{R}^3)} = (2\pi)^3\bigg\|\frac{\overline{\psi}(v^{-1}(\cdot))}{\sqrt{1-t^2}}f\big(\bar{s}v^{-1}(\cdot)s\big)\bigg\|^2_{L^2(B^3)}.$$

Returning to the unit sphere S^3 by setting $\phi=\arcsin t$, we obtain

$$\|V_\psi f\|^2 = 8\pi^3\int_{Spin(4)}\int_{S^3_+}\frac{|\overline{\psi}(\Lambda(\theta,\alpha,\phi))|^2}{\cos\phi}\big|f\big(\bar{s}\Lambda(\theta,\alpha,\phi)s\big)\big|^2\,d\phi\,d\alpha\,d\theta\,d\mu(s).$$

By Fubini's theorem and using the invariance of the measure $d\mu(s)$ (see [29]) we get

$$\begin{aligned}\|V_\psi f\|^2 &= 8\pi^3\int_{S^3_+}\frac{|\overline{\psi}(\Lambda(\theta,\alpha,\phi))|^2}{\cos\phi}\int_{Spin(4)}\big|f\big(\bar{s}\Lambda(\theta,\alpha,\phi)s\big)\big|^2\,d\mu(s)\,d\phi\,d\alpha\,d\theta\\ &= 8\pi^3\int_{S^3_+}\frac{|\overline{\psi}(\Lambda(\theta,\alpha,\phi))|^2}{\cos\phi}8\pi^2\|f\|^2_{L^2(S^3)}\,d\phi\,d\alpha\,d\theta\\ &= 64\pi^5\int_{S^3_+}\frac{|\overline{\psi}(\Lambda(\theta,\alpha,\phi))|^2}{\cos\phi}\,d\phi\,d\alpha\,d\theta\|f\|^2_{L^2(S^3)}. \qquad \square\end{aligned}$$

If ψ fulfills (5), then ψ is called *admissible* with respect to σ. In this case, (ψ,σ) is called a *strictly admissible pair*.

As a consequence, the proposed windowed Fourier transform can be inverted via its adjoint $V^*_\psi/\sqrt{C_\psi}$ (cf. formula (65) in [29]).

Corollary 1 *(Reconstruction). Any $f\in L_2(S^3)$ can be reconstructed from its Gabor transform by*

$$f(q)=\frac{1}{C_\psi}\int_{Spin(4)}\int_{\mathbb{R}^3}V_\psi f(s,p)e^{-i\langle\bar{s}ps,q\rangle}\psi(sq\bar{s})\,dp\,d\mu(s).$$

2.2. Reproducing kernel Hilbert space and frame theory

In order to obtain Gabor frames we will employ coorbit space theory. To keep notations and technicalities of coorbit space theory at a reasonable level, we only sketch the main ingredients and review the main conditions that need to be verified for our specific situation.

Assume that (ψ,σ) is a strictly admissible pair. In order to establish frames in $L_2(S^3)$, coorbit space theory restricted to Hilbert spaces suggests the following procedure. We first have to establish a correspondence principle between $L_2(S^3)$ and an associated reproducing kernel Hilbert space (as a subspace of $L_2(Spin(4)\times\mathbb{R}^3)$). Then a suitable discretization $\{x_\gamma\}_{\gamma\in\Gamma}\subset Spin(4)\times\mathbb{R}^3$ must be chosen in order to derive frames.

Let us define the kernel function

$$R(l,h)=\big\langle\psi, U\big(\sigma(h)\sigma(l)^{-1}\big)\psi\big\rangle = V_\psi\big(U\big(\sigma(l)^{-1}\big)\psi\big)(h)$$

and the reproducing kernel Hilbert space

$$\mathcal{M}_2 := \big\{F \in L_2\big(Spin(4) \times \mathbb{R}^3\big)\colon \big\langle F, R(h,\cdot)\big\rangle = F\big\}.$$

The following correspondence principle holds true, see [8].

Proposition 1 *(Correspondence principle). Let U be a square integrable representation of the Euclidean group $Spin(4) \ltimes \mathbb{R}^4$ modulo (H,σ) on $L_2(S^3)$ with a strictly admissible pair (ψ,σ). Then V_ψ is a bijection of $L_2(S^3)$ onto the reproducing kernel Hilbert space $\mathcal{M}_2$.*

The next step is to derive frames for this space. The major tool in [7,8] is the construction of a bounded partition of unity corresponding to some $\mathcal{U}$-dense and relatively separated sequence $\{x_\gamma\}_{\gamma\in\Gamma} \subset X$ that represents then our desired discretization. A sequence $\{x_\gamma\}_{\gamma\in\Gamma}$ is called $\mathcal{U}$-*dense* if $\bigcup_{\gamma\in\Gamma} \sigma(x_\gamma)\mathcal{U} \supset \sigma(X)$ for some relatively compact neighborhood $\mathcal{U}$ of the identity $e \in Spin(4)\times\mathbb{R}^3$ with non-void interior and is called *relatively separated*, if $\sup_{\eta\in\Gamma} \sharp\{\gamma \in \Gamma\colon\ \sigma(x_\gamma)L \cap \sigma(x_\eta)L \neq \emptyset\} \leqslant C_L$ for all compact subsets $L \subset Spin(4)\times\mathbb{R}^3$. It can be proved that there always exist such sequences $\{x_\gamma\}_{\gamma\in\Gamma}$ for all locally compact groups, all closed subspaces H and all relatively compact neighborhoods $\mathcal{U}$ of e with non-void interior. Note that the subsets $X_\gamma := \{x \in X\colon\ \sigma(x) \in \sigma(x_\gamma)\mathcal{U}\}$ clearly form a covering of X with uniformly finite overlap.

In [7] a judicious discretization for rotations/translations was suggested based on an Euler angle parametrization of the sphere (but no specific choice was made, just conditions were verified). In there, the discrete frequencies were obtained by a straightforward uniform spacing of the Euclidean space. However, in the present case of $Spin(4)$ that would imply dealing with 6 parameters. The high computational cost involved forces us to implement a reduction of our parameter space to $Spin(3) \equiv S^3$. This reduction will be described in the next section.

In this paper, we propose to obtain a translation grid by applying a direct spherical discretization method that was elaborated in [21]. This method yields a 'fair' grid, i.e., a near-uniformly spaced spherical grid (up to certain precision of the uniform spacing). To obtain the spherical grid points, a subdivision scheme is developed that is based on the spherical kinematic mapping. This goes as follows: in a first step an elliptic linear congruence is discretized by the icosahedral discretization of the unit sphere S^3. Then the resulting lines of the elliptic three-space are discretized such that the difference between the maximal and minimal elliptic distance between neighboring grid points becomes minimal.

Assume the grid is chosen as mentioned above and fulfills the requirements. Then the problem arises under which conditions a function f has an atomic decomposition and the set $\{U(\sigma(x_\gamma))\psi\colon\ \gamma\in\Gamma\}$ forms a frame. To answer this question, we have to define the $\mathrm{osc}_{\mathcal{U}}$-kernel

$$\mathrm{osc}_{\mathcal{U}}(l,h) := \sup_{u\in\mathcal{U}} \big|\big\langle \psi, U\big(\sigma(l)\sigma(h)^{-1}\big)\psi - U\big(u^{-1}\sigma(l)\sigma(h)^{-1}\big)\psi\big\rangle_{L_2(S^3)}\big|.$$

On the basis of $\mathrm{osc}_{\mathcal{U}}$ we have the following two major statements at our disposal, see [7,8].

Theorem 1 *(Atomic decomposition). Assume that the relatively compact neighborhood $\mathcal{U}$ of the identity in $Spin(4)\times\mathbb{R}^3$ can be chosen so small that*

$$\int_X \mathrm{osc}_{\mathcal{U}}(l,h)\,d\mu(l) < \vartheta \quad \text{and} \quad \int_X \mathrm{osc}_{\mathcal{U}}(l,h)\,d\mu(h) < \vartheta \tag{7}$$

with $\vartheta < 1$. Let $\{x_\gamma\}_{\gamma\in\Gamma}$ be a $\mathcal{U}$-dense, relatively separated family. Then $L_2(S^3)$ admits the following atomic decomposition: if $f \in L_2(S^3)$, then there exists a sequence $c = (c_\gamma)_{\gamma\in\Gamma}$ such that f can be represented as

$$f = \sum_{\gamma\in\Gamma} c_\gamma U\big(\sigma(x_\gamma)\big)\psi,$$

where $c \in \ell_2$ and $\|c\|_{\ell_2} \leqslant A\|f\|_{L_2(S^3)}$. Moreover, if $c \in \ell_2$, then $f = \sum_{\gamma\in\Gamma} c_\gamma U(\sigma(x_\gamma))\psi \in L_2(S^3)$ and $\|f\|_{L_2(S^3)} \leqslant B\|c\|_{\ell_2}$.

Theorem 2 *(Frames). Impose the same assumptions as in Theorem 1 with the more restrictive condition*

$$\int_X \mathrm{osc}_{\mathcal{U}}(l,h)\,d\mu(l) < \frac{\vartheta}{C_\psi} \quad \text{and} \quad \int_X \mathrm{osc}_{\mathcal{U}}(l,h)\,d\mu(h) < \frac{\vartheta}{C_\psi} \tag{8}$$

where $\vartheta < 1$. Then the set

$$\big\{\psi_\gamma := U\big(\sigma(x_\gamma)\big)\psi\colon\ \gamma\in\Gamma\big\}$$

is a frame for $L_2(S^3)$. This means that

1. $f \in L_2(S^3) \Leftrightarrow \{\langle f,\psi_\gamma\rangle\}_{\gamma\in\Gamma} \in \ell_2$,
2. *there exists constants $0 < A \leqslant B < \infty$ such that*

$$A\|f\|_{L_2(S^3)} \leqslant \big\|\big\{\langle f,\psi_\gamma\rangle\big\}_{\gamma\in\Gamma}\big\|_{\ell_2} \leqslant B\|f\|_{L_2(S^3)},$$

3. *there exists a bounded, linear synthesis operator $S : \ell_2 \to L_2(S^3)$ such that $S(\{\langle f,\psi_\gamma\rangle\}_{\gamma\in\Gamma}) = f$.*

2.3. Verification of frame conditions

In order to establish Theorems 1 and 2 we have to verify conditions (7) and (8). To simplify technicalities and later therewith the computational complexity, we reduce the number of parameters in $X = Spin(4) \times \mathbb{R}^3$ (nine parameters) by restricting ourselves to zonal window functions. Thus, we can consider the factorization of $Spin(4)$ by $Spin(3)$, i.e. $Spin(4)/Spin(3) \simeq S^3$ which allows us to consider $L_2(S^3 \times \mathbb{R}^3)$.

Let us now check condition (7) in Theorem 1. Note that condition (8) in Theorem 2 can be verified analogously and is, therefore, omitted. Let $h = (s_1, p), l = (s_2, r) \in G/H$ with $p = (p_1, p_2, p_3, 0)$ and $r = (r_1, r_2, r_3, 0)$ be given. Then, by (2) and (1) we have

$$\sigma(h)\sigma(l)^{-1} = (s_1, p) \circ (\overline{s_2}, -\overline{s_2} r s_2) = (s_1 \overline{s_2}, p - s_1 \overline{s_2} r s_2 \overline{s_1}).$$

Consider the neighborhood of e given by $\mathcal{U}_\epsilon := \{u = (s_u, p_u)\colon\ s_u \in C_\epsilon,\ \ p_u \in [-\epsilon, \epsilon]^3\} \subset S^3 \times \mathbb{R}^3$, with $C_\epsilon = \{\Lambda(\theta, \alpha, \phi)\colon\ \theta \in [0, 2\pi),\ \ \alpha \in [0, \pi),\ \ \phi \in [0, \epsilon\pi)\}$ being a spherical ϵ-cap. The sampling grid $\{x_\gamma\}_{\gamma \in \Gamma}$ can be specified by $x_\gamma = x_{\gamma(j,m)} = (s_j, p_m)$, where s_j correspond to the grid points generated by the previously mentioned subdivision scheme in [21] and p_m are uniformly spaced points in $\mathbb{R}^3$. For each chosen ϵ the sampling density can be accordingly adjusted (on S^3 by the subdivision scheme and in $\mathbb{R}^3$ simply by a finer and finer spacing) such that $X_\gamma = \{x \in X\colon\ \sigma(x) \in \sigma(x_\gamma)\mathcal{U}\}$ forms a covering of X that is $\mathcal{U}$-dense and relatively separated. To show that the oscillation condition (7) can be satisfied we proceed in a similar way as in [8]. With the help of

$$\sigma(h)\sigma(l)^{-1}u = \big(s_1 \overline{s_2} s_u,\ p - s_1 \overline{s_2}(r - p_u) s_2 \overline{s_1}\big)$$

we obtain

$$\begin{aligned}
&\int_{S^3} \big(U\big(\sigma(l)\sigma(h)^{-1}\big)\psi(q)\overline{\psi}(q) - U\big(\sigma(l)\sigma(h)^{-1}u\big)\psi(q)\overline{\psi}(q)\big)\, dS_q \\
&\quad = \int_{S^3} \big(e^{i\langle q, p - s_1\overline{s_2} r s_2 \overline{s_1}\rangle}\psi(s_2\overline{s_1} q s_1 \overline{s_2})\overline{\psi}(q) - e^{i\langle q, p - s_1\overline{s_2}(r - p_u)s_2\overline{s_1}\rangle}\psi(s_2\overline{s_1} s_u q \overline{s_u} s_1 \overline{s_2})\overline{\psi}(q)\big)\, dS_q \\
&\quad = \int_{S^3_+} e^{i\langle q, p - s_1\overline{s_2} r s_2 \overline{s_1}\rangle}\big[\big(\psi(s_2\overline{s_1} q s_1 \overline{s_2}) - \psi(s_2\overline{s_1} s_u q \overline{s_u} s_1 \overline{s_2})\big)\overline{\psi}(q) \\
&\qquad + \big(1 - e^{i\langle q, s_1\overline{s_2} p_u s_2 \overline{s_1}\rangle}\psi(s_2\overline{s_1} s_u q \overline{s_u} s_1 \overline{s_2})\overline{\psi}(q)\big)\big]\, dS_q.
\end{aligned}$$

This leads to

$$\begin{aligned}
\operatorname{osc}_{\mathcal{U}}(l, h) \leqslant \sup_{u \in \mathcal{U}} &\left| \int_{S^3_+} e^{i\langle q, p - s_1\overline{s_2} r s_2 \overline{s_1}\rangle}\big(\psi(s_2\overline{s_1} q s_1 \overline{s_2}) - \psi(s_2\overline{s_1} s_u q \overline{s_u} s_1 \overline{s_2})\big)\overline{\psi}(q)\, dS_q \right| \\
&+ \sup_{u \in \mathcal{U}} \left| \int_{S^3_+} e^{i\langle q, p - s_1\overline{s_2} r s_2 \overline{s_1}\rangle}\big(1 - e^{i\langle q, s_1\overline{s_2} p_u s_2 \overline{s_1}\rangle}\big)\psi(s_2\overline{s_1} s_u q \overline{s_u} s_1 \overline{s_2})\overline{\psi}(q)\, dS_q \right|.
\end{aligned}$$

To bound $I := \int_X \operatorname{osc}_{\mathcal{U}}(l, h)\, d\mu(h)$ we apply the last estimate and we get

$$I \leqslant \int_{S^3} (I_1 + I_2)\, d\mu(s_1)$$

where

$$I_1 := \int_{\mathbb{R}^3} \sup_{u \in \mathcal{U}} \left| \int_{S^3_+} e^{i\langle q, p - s_1\overline{s_2} r s_2 \overline{s_1}\rangle}\big[\psi(s_2\overline{s_1} q s_1 \overline{s_2}) - \psi(s_2\overline{s_1} s_u q \overline{s_u} s_1 \overline{s_2})\big]\overline{\psi}(q)\, dS_q \right| dp,$$

and

$$I_2 := \int_{\mathbb{R}^3} \sup_{u \in \mathcal{U}} \left| \int_{S^3_+} e^{i\langle q, p - s_1\overline{s_2} r s_2 \overline{s_1}\rangle}\big(1 - e^{i\langle q, s_1\overline{s_2} p_u s_2 \overline{s_1}\rangle}\big)\psi(s_2\overline{s_1} s_u q \overline{s_u} s_1 \overline{s_2})\overline{\psi}(q)\, dS_q \right| dp.$$

We first consider I_1. Projecting q onto the unit ball B^3 yields

$$I_1 := \int_{\mathbb{R}^3} \sup_{u\in\mathcal{U}} \Big| \int_{B^3} e^{i\langle x(t,\theta,\alpha),\underline{p}\rangle} e^{-i\langle x(t,\theta,\alpha), s_1\overline{s_2} r s_2\overline{s_1}\rangle} \big[\psi\big(s_2\overline{s_1} v^{-1}\big(x(t,\theta,\alpha)\big) s_1\overline{s_2}\big) - \psi\big(s_2\overline{s_1} s_u v^{-1}\big(x(t,\theta,\alpha)\big)\overline{s_u} s_1\overline{s_2}\big)\big]\overline{\psi}\big(x(t,\theta,\alpha)\big) \frac{t^2\sin\alpha}{\sqrt{1-t^2}}\, dt\, d\theta\, d\alpha \Big| d\underline{p}.$$

Introducing the functions

$$g(t,\theta,\alpha) = \begin{cases} \frac{e^{-i\langle x(t,\theta,\alpha), s_1\overline{s_2} r s_2\overline{s_1}\rangle}\sqrt{\overline{\psi}(x(t,\theta,\alpha))}}{\sqrt{1-t^2}}, & t\in[0,1],\ \theta\in[-\pi,\pi],\ \alpha\in[0,\pi[, \\ 0, & \text{otherwise,} \end{cases}$$

and

$$w_{s_u}(t,\theta,\alpha) = \begin{cases} [\psi(s_2\overline{s_1} v^{-1}(x(t,\theta,\alpha)) s_1\overline{s_2}) \\ \quad - \psi(s_2\overline{s_1} s_u v^{-1}(x(t,\theta,\alpha))\overline{s_u} s_1\overline{s_2})]\sqrt{\overline{\psi}(x(t,\theta,\alpha))}, & t\in[0,1],\ \theta\in[-\pi,\pi],\ \alpha\in[0,\pi[, \\ 0, & \text{otherwise,} \end{cases}$$

we can rewrite I_1 as

$$\begin{aligned} I_1 &= \int_{\mathbb{R}^3} \sup_{u\in\mathcal{U}} \Big| \int_{-\infty}^{\infty}\int_{0}^{\pi}\int_{-\pi}^{\pi} e^{i\langle x(t,\theta,\alpha),\underline{p}\rangle} w_{s_u}(t,\theta,\alpha) g(t,\theta,\alpha) t^2\sin\alpha\, d\theta\, d\alpha\, dt \Big| d\underline{p} \\ &\leqslant \int_{\mathbb{R}^3} \sup_{u\in\mathcal{U}} \big|\big(\mathcal{F}(w_{s_u}) * \mathcal{F}g\big)(\underline{p})\big|\, d\underline{p} \\ &\leqslant \int_{\mathbb{R}^3} \sup_{u\in\mathcal{U}} \int_{\mathbb{R}^3} \big|(\mathcal{F}(w_{s_u})(\xi)\big|\big|\mathcal{F}g\big((\underline{p}) - \xi\big)\big|\, d\xi\, d\underline{p}. \end{aligned} \tag{9}$$

Observe that w_{s_u} has compact support. Now, if we choose ψ smooth enough, i.e. $w_{s_u}\in C^k(\mathbb{R}^3)$, $k\geqslant 4$, and $g\in L_1$, then $\lim_{s_u\to \mathrm{id}} w_{s_u}^{(k)} = 0$ and by dominated convergence we get

$$\lim_{s_u\to\mathrm{id}} \big\| w_{s_u}^{(k)} \big\|_{L_1} = 0.$$

This also implies that

$$\lim_{s_u\to\mathrm{id}} \big\| \mathcal{F}\big(w_{s_u}^{(k)}\big) \big\|_{L_\infty} = 0.$$

Therefore, by using

$$\mathcal{F}\big(w_{s_u}^{(k)}\big)(\xi) = (-i\xi)^k \mathcal{F}(w_{s_u})(\xi)$$

we have

$$\big|\mathcal{F}\big(w_{s_u}^{(k)}\big)(\xi)\big| \leqslant \big(1+|\xi|\big)^{-k} c(s_u), \tag{10}$$

where $c(s_u)$ denotes a continuous function with $\lim_{s_u\to\mathrm{id}} c(s_u) = 0$. Inserting (10) into (9), we obtain

$$\begin{aligned} I_1 &\leqslant \int_{\mathbb{R}^3} \sup_{u\in\mathcal{U}} c(s_u) \int_{\mathbb{R}^3} \big(1+|\xi|\big)^{-r} \big|\mathcal{F}g(\underline{p}-\xi)\big|\, d\xi\, d\underline{p} \\ &\leqslant \big\|\mathcal{F}(g)\big\|_{L_1} \sup_{s_u\in C_\epsilon} c(s_u) \int_{\mathbb{R}^3} \big(1+|\xi|\big)^{-r} d\xi \\ &\leqslant C \sup_{s_u\in C_\epsilon} c(s_u). \end{aligned}$$

This expression becomes arbitrary small for sufficient small ϵ. For the second integral I_2 the function w_{p_u} is given by $(1 - e^{i\langle\omega, s_1\overline{s_2} p_u s_2\overline{s_1}\rangle})\sqrt{\overline{\psi}(q)}$. Hence, imposing the same regularity condition on ψ as in the estimate of I_1 one gets a similar result.

3. Inversion of the Radon transform

This section is concerned with the determination of the orientation density function f (ODF) of a polycrystalline specimen from given pole density data. The major assumption is that f can be sufficiently well represented by the spherical Gabor frames introduced in the previous section. Then the remaining task is to solve a discretized operator equation, i.e., to determine the synthesis coefficients (or the atomic representation) of f. As the data are allowed to be noisy (which is for any practical measurement process impossible to avoid), the Radon operator must be considered between $L_2(S^3)$ and $L_2(S^2 \times S^2)$ and is, therefore, ill-posed (and not as the operator properties suggest a map with negative order between Sobolev spaces (see [3])). Consequently, we are faced with regularization issues, i.e., the inversion procedure must be stabilized against the influence of noise.

Before we enter into the issue let us give a short remark on the spherical Radon transform.

3.1. Crystallography and the spherical Radon transform

The orientation of an individual crystal is assumed to be unique and given by the rotation $q \in SO(3)$ which maps the specimen referential system K_s into coincidence with a coordinate system K_c fixed to the crystal, $q : K_s \mapsto K_c$. Hence the coordinates of the initial direction represented by $x \in S^2 \subset \mathbb{R}^3$ (w.r.t. the crystal coordinate system K_c) will be related to the ones of the final direction represented by $y \in S^2$ (w.r.t. the coordinate system K_s) by $y = \bar{q}xq$. With other words we assume that a crystal is uniquely determined by its invariance group (space group) $G \subset O(3) \times T(3)$. We are here interested in the part which corresponds to a subgroup (crystallographic group) $G_p := G/T(3) \subset O(3)$. A non-negative, integrable (possibly normalized) function

$$f : O(3)/G_p \mapsto \mathbb{R}_+$$

is called an orientation density function (ODF). The determination of such an ODF is called quantitative texture analysis. The ODF f can only be measured in an indirect way via the pole density function $\tilde{P}(x, y) = \frac{1}{2}((Rf)(x, y) + (Rf)(-x, y))$, there is, by means of two spherical Radon transforms of the orientation density function f [25,6]. The principle problem consists in how to determine the ODF from the measurements (pole figures).

Definition 1 *(Spherical Radon transform).* (See [6].) Let f belong to $L_1(S^3)$. We define the spherical Radon transform of f as the mean over all rotations q mapping the direction $x \in S^2$ into $y \in S^2$ and we write

$$\begin{aligned}(Rf)(x, y) &:= \frac{1}{2\pi} \int\limits_{\{q \in S^3 :\ y = \bar{q}xq\}} f(q)\, dq \\ &= \frac{1}{2\pi} \int\limits_0^{2\pi} f\big(q(x, y, t)\big)\, dt,\end{aligned} \tag{11}$$

where $q(x, y, t) = (\cos\frac{\eta}{2} + \frac{x\times y}{\|x\times y\|} \sin\frac{\eta}{2}) \cos t + \frac{x+y}{\|x+y\|} \sin t$, with $\eta = \arccos(\langle x, y\rangle)$, denotes the great circle in S^3 of all unit quaternions q which rotates $x \in S^2$ into $y \in S^2$.

Note that the invariant Haar measure in (11) is uniquely defined by the assumption that the measurements should be independent of the choices of the coordinate systems K_c, K_s.

3.2. Inversion by accelerated steepest descent and ℓ_1-projections

In this section, we address the problem of computing an approximation of a solution to the linear problem $Rf = g$. As already mentioned, we have to consider R as a map between $L_2(S^3)$ and $L_2(S^2 \times S^2)$ with $\|g - g^\delta\| \leqslant \delta$. Therefore, we are faced with the problem of ill-posedness (in the sense of a discontinuous dependence of the solution on the data) and therefore with regularization issues.

The goal is to propose an iterative procedure for deriving an approximation to the solution of the ill-posed inverse problem. Representing the solution of the inverse problem by the established Gabor frame $\{\psi_\gamma :\ \gamma = \gamma(j, m) \in \Gamma\} \subset L_2(S^3)$, i.e.

$$f = \sum_{\gamma \in \Gamma} c_\gamma \psi_\gamma,$$

the problem results in finding a sequence $\{c_\gamma\}_{\gamma \in \Gamma}$. For the Gabor frame we may consider the analysis and synthesis operator (adjoint of analysis operator),

$$F : L_2\big(S^3\big) \to \ell_2(\Gamma) \quad \text{via } f \mapsto \big\{\langle f, \psi_\gamma\rangle\big\}_{\gamma\in\Gamma}, \qquad F^* : \ell_2(\Gamma) \to L_2\big(S^3\big) \quad \text{via } c \mapsto \sum_{\gamma\in\Gamma} c_\gamma \psi_\gamma.$$

Therefore, the inverse problem can be recast as follows: find a sequence $c \in \ell_2(\Gamma)$ such that

$$RF^*c = g.$$

Note that due to the redundancy of the Gabor frame, c needs not to be unique. The data might also be inexact (disturbed by noise), therefore we alternatively focus on minimizing the Gaussian discrepancy

$$\Delta(c) := \big\| g^\delta - RF^*c \big\|^2_{L_2(S^2\times S^2)}.$$

As mentioned in the first section, we consider scenarios in which we can assume that the vector c is sparse, i.e. c has only a few non-vanishing coefficients or can be nicely approximated by a small number of coefficients. One well-understood approach to involve a sparsity constraint is given by adding an ℓ_1 penalty term to the Gaussian discrepancy leading to $\Delta(c) + \varrho\|c\|_{\ell_1(\Gamma)}$. The treatment of such functionals is not difficult to handle and was elaborated and successfully applied in several papers, see, e.g., [10–13,27]. However, the resulting iteration is known to converge usually quite slow and a detailed analysis of the characteristic dynamics of the corresponding thresholded Landweber iteration has shown that the algorithm converges initially relatively fast, then it overshoots the ℓ_1 penalty, and it takes very long to re-correct back. To circumvent this "external" detour it was proposed in [9,28] to force the iterates to remain within a particular ℓ_1 ball $B_K := \{x \in \ell_2(\Gamma);\ \|x\|_{\ell_1(\Gamma)} \leqslant K\}$. This leads to the constrained minimization approach

$$\min_{c\in B_K} \Delta(c). \tag{12}$$

To accelerate the resulting iteration we may apply techniques from standard linear steepest descent methods which is the use of adaptive step lengths. Therefore, a minimization of (12) results in a projected iteration with step length control,

$$c^{n+1} = P_{B_K}\left(c^n + \frac{\beta^n}{r} FR^*\big(g - RF^*c^n\big)\right), \tag{13}$$

where P_{B_K} denotes the orthogonal projection on B_K. The convergence of this method relies on a proper step length parameter rule for β^n. With respect to a sequence $\{c^n\}_{n\in\mathbb{N}}$ the parameter β^n must be chosen such that

$$\text{(B1)}\quad \bar\beta := \sup\big\{\beta^n; n\in\mathbb{N}\big\} < \infty \quad \text{and} \quad \inf\big\{\beta^n; n\in\mathbb{N}\big\} \geqslant 1,$$

$$\text{(B2)}\quad \beta^n \big\| RF^*c^{n+1} - RF^*c^n\big\|^2 \leqslant r\big\|c^{n+1} - c^n\big\|^2 \quad \forall n \geqslant n_0$$

are fulfilled, where the constant r is an upper bound for $\|RF^*\|^2$. Practically, the implementation of the proposed projected steepest descent algorithm is as follows:

Given	Operator R, some initial guess c^0, and K (sparsity constraint ℓ_1-ball B_K)
Initialization	$\|RF^*\|^2 \leqslant r$, set $q = 0.9$ (as an example)
Iteration	**for** $n = 0, 1, 2, \ldots$ **until** a preassigned precision/maximum number of iterations **1.** $\beta^n = C \cdot \sqrt{\frac{D(x^0)}{D(x^n)}}$, $C \geqslant 1$ (greedy guess) **2.** $c^{n+1} = P_{B_K}(c^n + \frac{\beta^n}{r} FR^*(g - RF^*c^n))$; **3.** verify (B2): $\beta^n \|RF^*c^{n+1} - RF^*c^n\|^2 \leqslant r\|c^{n+1} - c^n\|^2$ **if** (B2) is satisfied increase n and go to **1** **otherwise** set $\beta^n = q \cdot \beta^n$ and go to **2** **end**

When performing iteration (13) the main operating expense is due to the computation of FR^*RF^*. Therefore, an adaptive variant of the full iteration by involving adaptive matrix vector multiplications could significantly reduce the numerical complexity. Unfortunately, the matrix FR^*RF^* belongs neither to the Jaffard nor to the Lemarie class. Therefore, so far established adaptive strategies for operator equations cannot be applied in a straightforward way as done in the Euclidean situation, see [23]. Nevertheless, efficient strategies for computing the matrix entries are possible and allow thrifty linear approximation techniques.

3.3. Efficient computation of matrix entries

In this section we discuss the efficient calculation of the matrix FR^*RF^*. Its entries read as

$$\langle R\psi_{j,m}, R\psi_{j',m'}\rangle_{L_2(S^2\times S^2)} = \int_{S^2}\int_{S^2} R\psi_{j,m}(x,y)\overline{R\psi_{j',m'}(x,y)}\,dy\,dx. \tag{14}$$

In order to simplify the practical calculations we will consider ψ to be a zonal window function with support on the spherical cap $U_h = \{q \in S^3\colon\ q_0 \geqslant h\}$, for some $h \in]0,1[$. As an immediate consequence the parameter space is reduced to $X = S^3 \times \mathbb{R}^3$ and the action $sq\bar{s}$, $s \in Spin(4)$ can be replaced by the left translation action on S^3 defined by $\bar{s}q$, where $s \in S^3$. This is a left transitive action on S^3 such that the rotations from $Spin(3)$ around a point $q \in S^3$ are left out (see Appendix A.2). In this way the Radon transform of our atoms is given by

$$R\psi_{j,m}(x,y) = \frac{1}{2\pi}\int_0^{2\pi} e^{i\langle q(x,y,t),p_m\rangle}\psi\left(\overline{s_j}q(x,y,t)\right)dt, \tag{15}$$

with $s_j \in S^3$ and $p_m \in \mathbb{R}^3$.

In order to reduce the computational cost of (14) we will look now for symmetry properties of $R\psi_{j,m}$. Since

$$R\psi_{j,m}(x,y) = \frac{1}{2\pi}\int_0^{2\pi} e^{i\langle q(x,y,t),p_m\rangle}\psi\left(\overline{s_j}q(x,y,t)\right)dt \tag{16}$$

$$= \frac{1}{2\pi}\int_{-\pi}^{\pi} e^{i\langle q(x,y,t),p_m\rangle}\psi\left(\overline{s_j}q(x,y,t)\right)dt \tag{17}$$

then it is easy to see that $R\psi_{j,m}(-x,-y) = R\psi_{j,m}(x,y)$. Therefore, the inner products (14) reduce to

$$\begin{aligned}\langle R\psi_{j,m}, R\psi_{j',m'}\rangle_{L_2(S^2\times S^2)} &= 2\int_{S^2_+}\int_{S^2_+} R\psi_{j,m}(x,y)\overline{R\psi_{j',m'}(x,y)}\,dy\,dx\\ &\quad + 2\int_{S^2_+}\int_{S^2_-} R\psi_{j,m}(x,y)\overline{R\psi_{j',m'}(x,y)}\,dy\,dx,\end{aligned} \tag{18}$$

where S^2_+ and S^2_- represents the upper ($x_3 \geqslant 0$) and lower ($x_3 \leqslant 0$) hemispheres respectively.

The standard parametrization of great circles of S^3 by $q(x,y,t)$ as given in Definition 1 has a singularity in $y = -x$, that is, if $y = -x$ this parametrization is not well defined. Moreover, the gradient of $q(x,y,t)$ increases rapidly in a neighborhood of $y = -x$. To overcome this problem we will make a reparametrization of the great circles $q(x,y,t)$. By [20] we can reparametrize the great circle $q(x,y,t)$ introducing a vector $v \in S^2$ in the following way:

$$q(x,y,t) = q_4 v(t) q_3, \tag{19}$$

where

i) q_3 is any fixed quaternion such that $q_3 x\overline{q_3} = v$, with an arbitrarily given $v \in S^2$;
ii) $v(t) = \cos t/2 + v\sin t/2 \in S^3$ such that $v(t)v\overline{v(t)} = v$;
iii) $q_4 \in S^3$ is any fixed quaternion such that $q_4 v\overline{q_4} = y$.

Choosing $q_4 = \frac{y+v}{\|y+v\|}$ and $q_3 = \frac{x+v}{\|x+v\|}$ the new parametrization (19) is given by

$$q(x,y,t) = \frac{y+v}{\|y+v\|}(\cos t + v\sin t)\frac{x+v}{\|x+v\|}. \tag{20}$$

Thus, we partitioned (18) into

$$\langle R\psi_{j,m}, R\psi_{j',m'}\rangle_{L_2(S^2\times S^2)} = 2\mathcal{I}_1 + 2\mathcal{I}_2 + 2\mathcal{I}_3, \tag{21}$$

where

$$\mathcal{I}_1 = \int_{S^2_+}\int_{S^2_+} R\psi_{j,m}(x,y)\overline{R\psi_{j',m'}(x,y)}\,dy\,dx, \tag{22}$$

$$\mathcal{I}_2 = \int_{S^2_+:x_1\geqslant 0}\int_{S^2_-} R\psi_{j,m}(x,y)\overline{R\psi_{j',m'}(x,y)}\,dy\,dx, \tag{23}$$

$$\mathcal{I}_3 = \int_{S^2_+:x_1\leqslant 0}\int_{S^2_-} R\psi_{j,m}(x,y)\overline{R\psi_{j',m'}(x,y)}\,dy\,dx. \tag{24}$$

For each integral we will consider a new parametrization (20) with $v \in S^2$ chosen in such way that the singularities $x = -v$ and $y = -v$ are far away from the region of integration. For $\mathcal{I}_1$ we choose $v = (0,0,1)$, for $\mathcal{I}_2$ we choose $v = (\frac{\sqrt{2}}{2}, 0, -\frac{\sqrt{2}}{2})$ and for $\mathcal{I}_3$ we choose $v = (-\frac{\sqrt{2}}{2}, 0, -\frac{\sqrt{2}}{2})$. This leaves us with one major problem: how to calculate efficiently an integral of type

$$\int e^{i\langle k, q(\theta,\phi,\alpha,\beta,t)\rangle} f\big(q(\theta,\phi,\alpha,\beta,t)\big)\,d\alpha\,d\beta\,d\theta\,d\phi\,dt \tag{25}$$

with $k = (k_1,\dots,k_4)$, $q = (q_1,\dots,q_4)$, $q_i : R^5 \mapsto R$ which is a multidimensional integral of highly oscillatory type.

There are several methods in the literature, such as Fillon-type or Leray-type methods. But in order to apply these method we have to overcome one problem. Usually, in these methods the exponent is linear, while here it is non-linear. An attempt to linearize it could work, but it would create a huge number of individual integrals to compute which is difficult to implement.

A way out is to use so-called adaptive multiscale local Fourier bases (see [1,2,19]). These bases are generalizations of Malvar–Coifman–Meyer (MCM) wavelets. The basic idea is to use so-called bell functions b_i which provide a partition of unity, i.e. we have a subdivision of our interval $[0, 2\pi]$ into M subintervals I_i where each bell function is defined in three adjacent intervals and given by

$$b_i(x) = \begin{cases} \frac{1}{2}(1 + \sum_{l=0}^{i-1} g_l \sin((n+1)\pi x)), & -\frac{1}{2} \leqslant x \leqslant \frac{1}{2}, \\ \frac{1}{2}(1 + \sum_{l=0}^{i-1} (-1)^l g_l \cos((n+1)\pi x)), & \frac{1}{2} \leqslant x \leqslant \frac{3}{2}, \\ 0, & \text{otherwise.} \end{cases}$$

Hereby, g_l are solutions of a linear systems and tabulated in [19]. As remarked before, we have $\sum_{i=1}^{M} b_i(x) = 1$.

These bell functions allow us to introduce our local Fourier basis by

$$u^l_n(\theta,\phi,\alpha,\beta,t) = C^{l_1}_{n_1}(\alpha) C^{l_2}_{n_2}(\beta) C^{l_3}_{n_3}(\theta) C^{l_4}_{n_4}(\phi) C^{l_5}_{n_5}(t)$$

with $C^{l_i}_{n_i}(\cdot) = b_{l_i}(\cdot)(\frac{2}{a_{l_i+1}-a_{l_i}})^{1/2} \sin((n_i+\frac{1}{2})\pi \frac{\cdot - a_{l_i}}{a_{l_i+1}-a_{l_i}})$.

The application of these LFB's means that we have to calculate the Fourier coefficients

$$A_{n,l} = \int e^{i\langle k, q(\theta,\phi,\alpha,\beta,t)\rangle} u^l_n(\theta,\phi,\alpha,\beta,t)\,d\alpha\,d\beta\,d\theta\,d\phi\,dt,$$

$$B_{n,l} = \int f\big(q(\theta,\phi,\alpha,\beta,t)\big) u^l_n(\theta,\phi,\alpha,\beta,t)\,d\alpha\,d\beta\,d\theta\,d\phi\,dt,$$

separately. The integral is then given by $\sum_{n,l} A_{n,l} B_{n,l}$.

The calculation of the Fourier coefficients can be done either by corrected trapezoidal rule/Richardson interpolation (taking into account the support of the bell functions, but it requires caution with respect to the number of points one needs, see [1], Table 2 on p. 7) or by FFT (see [19]). In the case at hand, we will use FFT.

Furthermore, we need to study the sparsity condition by Averbuch et al., for both $B_{n,l}$ and $A_{n,l}$ in order to determine how many coefficients are really required (see [1], pp. 14–19). Let us consider our integral in the more shortened form

$$\int e^{i\langle k, q(\phi_i)\rangle} f(\phi_i)\,d\phi_1 \dots d\phi_5.$$

For simplification we write just ϕ_i for all our variables. To apply our method we develop our kernel in terms of LFB's:

$$\int e^{i\langle k, q(\phi_i)\rangle} C_1(\phi_1)\dots C_5(\phi_5)\,d\phi_1\dots d\phi_5. \tag{26}$$

Following the same ideas as in [2] we can study the sparsity of this development. The principal condition for the sparsity considerations is that

$$\left|\frac{\partial^{|\mu|}}{\partial\phi_1^{\mu_1}\dots\partial\phi_5^{\mu_5}}q(\phi_1,\dots,\phi_5)\right|\leqslant C, \tag{27}$$

i.e. the derivatives of order $|\mu|$ are bounded. Let us first remark that our function q satisfies for each subdivision the above condition, but with a constant C which will go to infinity when the total degree for the derivatives goes to infinity, i.e. getting worse with each derivation. Furthermore, we remark that we need at least two points per oscillation, i.e. $N=10\nu$ (for simplification we consider ν oscillations in each direction). This will result in $\sqrt{N}=\sqrt{10\nu}$ bell functions.

Now, using as rescaling for the bells the maximum frequency, i.e. $\nu=\max_{i=1,2,3}k_i$ we get via linearization for the coefficients (26)

$$\begin{aligned}
&\int e^{i\langle k,q(\phi_i)\rangle}C_1(\phi_1)\dots C_5(\phi_5)\,d\phi_1\dots d\phi_5\\
&\quad\approx e^{i\sum_{l=1}^3(\sum_{i=1}^3 k_i q_i(\phi^*)-\sum_{i=1}^3 k_i\frac{\partial q_i}{\partial\phi_l}(\phi^*)\phi_l^*)}\int e^{i(\sum_{i=1}^3 k_i\frac{\partial q_i}{\partial\phi_1}(\phi^*))\phi_1}\\
&\qquad\times e^{i(\sum_{i=1}^3 k_i\frac{\partial q_i}{\partial\phi_2}(\phi^*)),\phi_2}e^{i(\sum_{i=1}^4 k_i\frac{\partial q_i}{\partial\phi_3}(\phi^*))\phi_3}e^{i(\sum_{i=1}^4 k_i\frac{\partial q_i}{\partial\phi_4}(\phi^*))\phi_4}\\
&\qquad\times e^{i(\sum_{i=1}^4 k_i\frac{\partial q_i}{\partial\phi_5}(\phi^*))\phi_5}C_1(\phi_1)C_2(\phi_2)C_3(\phi_3)C_4(\phi_4)C_5(\phi_5)\,d\phi_1\,d\phi_2\,d\phi_3\,d\phi_4\,d\phi_5.
\end{aligned}$$

We collect all the exponentials together and denote the residual term (incl. Hessian) of the linearization by $H^{\nu_{k,k'}(\phi_1,\dots,\phi_5)}$. Using the rescaling of [1] (which corresponds to an independent affine transformation in each variable) we can view our integral as the Fourier transform of

$$\beta(\phi_1,\dots,\phi_5)=b(\phi_1)b(\phi_2)b(\phi_3)b(\phi_4)b(\phi_5)e^{iH^{\nu_{k,k'}(\phi_1,\dots,\phi_5)}}.$$

Now, we prove that there exists a constant C' such that

$$\left|H^{\nu}_{k,k'}(\phi_1,\dots,\phi_5)\right|\leqslant C'. \tag{28}$$

If this is true then we obtain

$$\left|\frac{\partial^{|\mu|}H^{\nu}_{k,k'}}{\partial_{\phi_1^{\mu_1}}\dots\partial_{\phi_5^{\mu_5}}}(\phi_1,\dots,\phi_5)\right|\leqslant\frac{C'}{(\sqrt{\nu})^{|\mu|}}$$

from the rescaling and the fact that at each derivative of q_i a $\sqrt{\nu}$ comes out. With other words the residual (Hessian) has a gradient of order $O(\frac{1}{\sqrt{\nu}})$.

This now allows us to get the result of Averbuch et al. [2, p. 18] in our case:

$$\left|\hat{\beta}(\xi_1,\dots,\xi_5)\right|\leqslant\frac{C_1}{1+\max_i|\xi_i|^{|\mu|}}.$$

Estimate (28) follows immediately from estimating the derivatives of the parametrization (cf. (20))

$$q(x,y,t)=\frac{y+v}{\|y+v\|}(\cos t+v\sin t)\frac{x+v}{\|x+v\|}.$$

Here we have to take into account the different nature of x, y on one side and t on the other. By straightforward calculations we get

$$\left\|\frac{\partial^{\mu}q(x,y,t)}{\partial x_1{}^{\mu_1}\dots\partial y_1{}^{\mu_4}\dots\partial t^{\mu_7}}\right\|\leqslant\frac{C_\mu}{\|x+v\|^{\mu_1+\mu_2+\mu_3}\|y+v\|^{\mu_4+\mu_5+\mu_6}}.$$

Let us remark that the denominator is always bounded, the bound growing with μ. Also, in the case of (22) we get the estimates $\|y+v\|\geqslant 1/2$ and $\|x+v\|\geqslant 1/2$, whereas for (23) and (24) we have $\|y+v\|\geqslant 2-\sqrt{2}$ and $\|x+v\|\geqslant 2-\sqrt{2}$.

For practical implementation we are interested in the Hessian, that is to say in the second derivatives. Here we can obtain a better estimate than above by directly using a suitable system of spherical coordinates $x=x(\theta,\phi)$ and $y=y(\alpha,\beta)$. The maximum will be reached by the derivatives $\frac{\partial^2 q}{\partial\phi^2}$ and $\frac{\partial^2 q}{\partial\beta^2}$. For these derivatives we get

$$\begin{aligned}
\left\|\frac{\partial^2 q}{\partial\phi^2}\right\|\leqslant{}&\frac{3|-v_1\cos\theta\cos\phi-v_2\sin\theta\cos\phi+v_3\sin\phi|^2}{\|v+x(\theta,\phi)\|^4}+\frac{|v_1\cos\theta\sin\phi+v_2\sin\theta\sin\phi+v_3\cos\phi|}{\|v+x(\theta,\phi)\|^2}\\
&+2\frac{|-v_1\cos\theta\cos\phi-v_2\sin\theta\cos\phi+v_3\sin\phi|}{\|v+x(\theta,\phi)\|^3}+\frac{1}{\|v+x(\theta,\phi)\|}
\end{aligned}$$

and

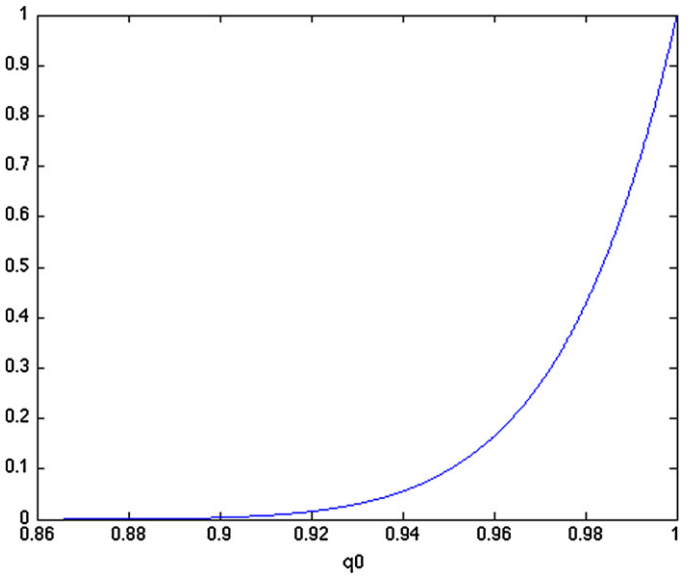

Fig. 1. Section of the radial Gabor atom ψ.

$$\left\|\frac{\partial^2 q}{\partial\beta^2}\right\| \leqslant \frac{3|-v_1\cos\alpha\cos\beta - v_2\sin\alpha\cos\beta + v_3\sin\beta|^2}{\|v+y(\alpha,\beta)\|^4} + \frac{|v_1\cos\alpha\sin\beta + v_2\sin\alpha\sin\beta + v_3\cos\beta|}{\|v+y(\alpha,\beta)\|^2} + 2\frac{|-v_1\cos\alpha\cos\beta - v_2\sin\alpha\cos\beta + v_3\sin\beta|}{\|v+y(\alpha,\beta)\|^3} + \frac{1}{\|v+y(\alpha,\beta)\|}.$$

The integrals for the entries in our matrix can now be calculated by

$$\sum_{n,l} A_{n,l}^{j} A_{n,l}^{j'} B_{n,l}^{m} B_{n,l}^{m'},$$

where the upper indices j, m are denoting the correspondence to the respective atom $\psi_{j,m}$, i.e. m the frequency index and j the index from the rotation grid. Due to the property $\langle R\psi_{j',m'}, R\psi_{j,m}\rangle = \overline{\langle R\psi_{j,m}, R\psi_{j',m'}\rangle}$ we only need to calculate $(JM^3)(1+JM^3)/2$ entries, where J denotes the number of translation/rotation grid point and M the number of frequency points. Using the same arguments as in Averbuch et al. ([1], Section 3.3, and [2], Section 3) we get that for the calculation of $A_{n,l}B_{n,l}$ we need at most $O(N^{5/2})$ coefficients. With $N = 10M$ (M-highest frequency, less than 2 points per oscillation would not work) we obtain

$$\big(JM^3\big)\big(1+JM^3\big)/2 \times O\big(M^{5/2}\big)$$

or, with other words, the complexity of the problem is of size $O(M^{17/2}J^2)$.

3.4. Crystallography and numerical experiments

For the numerical experiments we first have to specify the analyzing Gabor atoms. In the present example we limit ourselves to radial functions over the real axis where ψ is defined by

$$\psi(q) = \cos^6\big(2.6\arccos(q_0)\big), \quad \frac{\sqrt{3}}{2} \leqslant q_0 \leqslant 1,$$

see Fig. 1. If $q = \Lambda(\theta,\alpha,\phi)$, $\theta \in [0, 2\pi[$, $\alpha \in [0,\pi[$ and $\phi \in [0,\pi]$, where Λ is defined as in (6) then the Gabor atom reads as

$$\psi(\theta,\alpha,\phi) = \cos^6(2.6\phi), \quad \frac{\pi}{6} \leqslant \phi \leqslant \frac{\pi}{2}.$$

The corresponding admissibility constant is

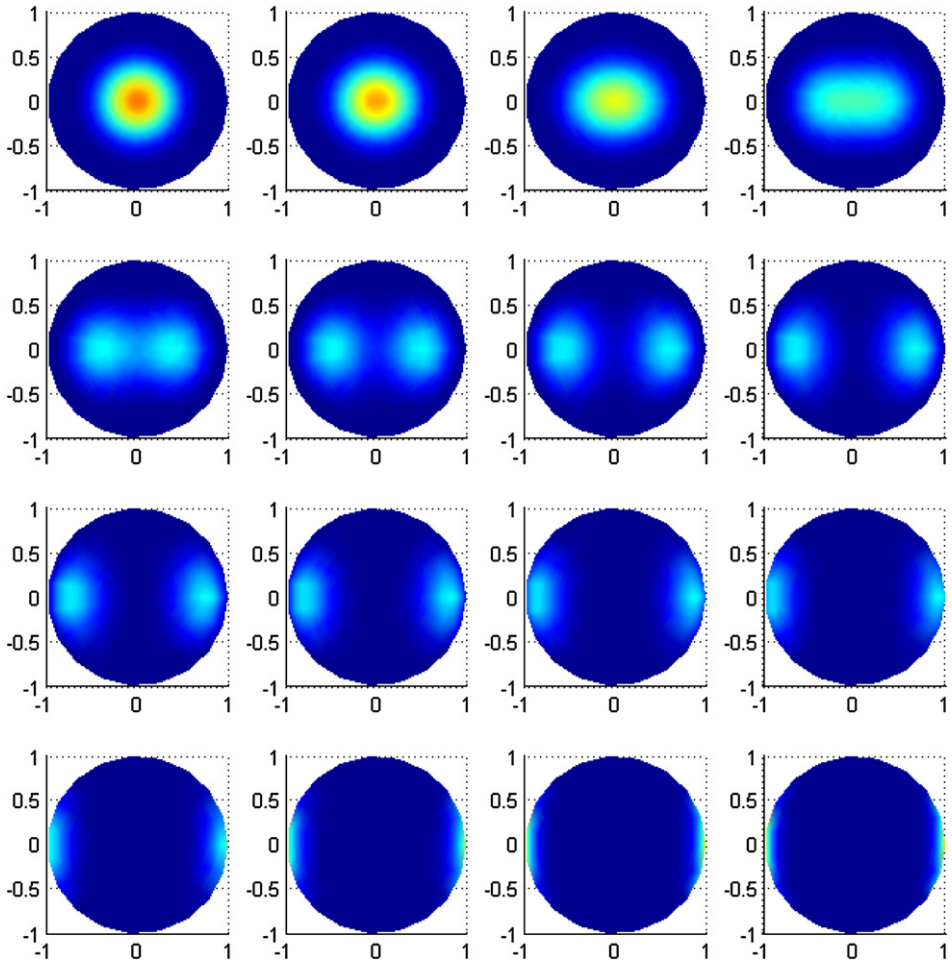

Fig. 2. Pole figures for the crystal configuration.

$$C_\psi = 64\pi^5 \int_0^{2\pi}\int_0^{\pi}\int_0^{\pi/2} \frac{|\psi(q(\theta,\alpha,\phi))|^2}{\cos\phi}\, d\phi\, d\alpha\, d\theta \approx 17.54532476\pi^7 \approx 52\,992.$$

The overlapping of the corresponding frame system is as follows. Consider the Gabor atom defined on the spherical cap

$$U_{\frac{\sqrt{3}}{2}} = \left\{ q \in S^3 \colon q_0 \geqslant \frac{\sqrt{3}}{2} \right\}.$$

This cap is centered on the real axis and has a size of $\frac{\pi}{6}$ radians.

Let us now define the associated frame grid. The rotations on S^3 are given by the 120 vertices of the 600-cell. This provides us with several advantages. Firstly, the vertices of the 600-cell represent a discrete subgroup of unit quaternions, the binary icosahedral group, a double covering of the icosahedral group. While the group itself is not crystallographic, 14 of the 32 crystallographic groups are subgroups of this group, like the cyclic groups generated by the various elements or D_3. Secondly, finer but still quasi-uniform grids can be created starting from this grid by subdivision schemes [21]. This also means that we can assume sparsity for the ODF's for these groups with respect to the rotation grid. While the observation on the grid provides just a necessary condition for sparsity we like to point out that to assume that our ODF is well-localized corresponds to similar modeling assumptions in the literature (e.g., see [26]). As the distance between two neighboring vertices of the 600-cell is $\frac{\pi}{5}$ then the overlapping between two caps is about $\frac{2\pi}{15}$. This gives a ratio of $\frac{4}{5}$ between the overlapping chosen and the maximum overlapping coincident with the distance between two neighboring vertices of the 600-cell.

For the frequency grid we choose a three-dimensional grid in $\mathbb{Z}_3 \cup \{(0,0,0)\}$ as follows:

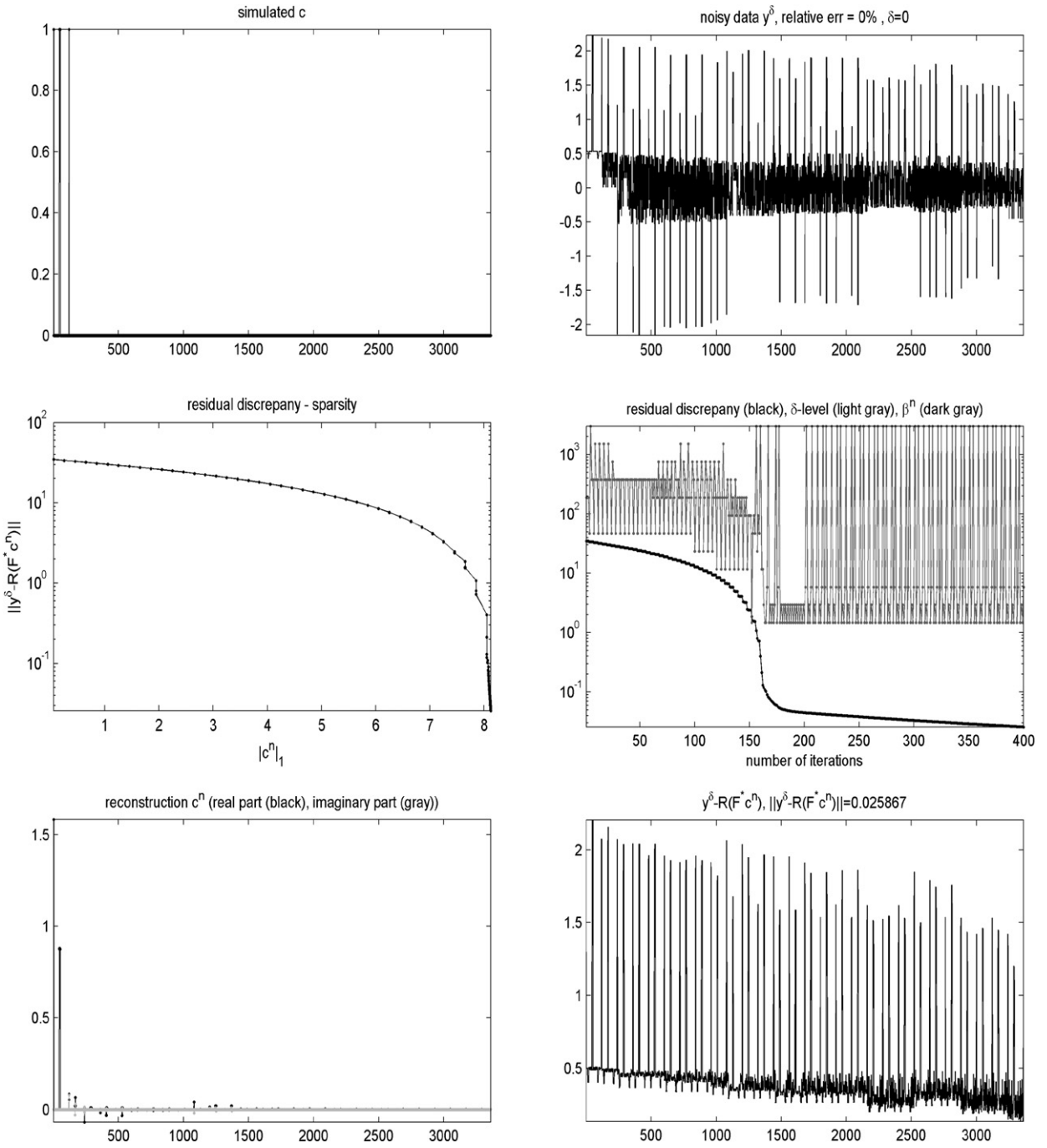

Fig. 3. Reconstruction process of iteration (13) for the noise-free scenario. From top left to bottom right: simulated sequence c, simulated data y^δ, residual discrepancy (L_2 norm)–sparsity (ℓ_1 norm) plot, residual discrepancy plot including step length control β^n and noise level δ, reconstructed sequence c^n (truncated after 400 iterations), residual error $y^\delta - R(F^* c^n)$.

$$\big\{(0,0,0),(1,1,1),(3,1,1),(1,3,1),(1,1,3),(3,3,1),(1,3,3),(3,1,3),(3,3,3),(6,1,1),$$
$$(1,6,1),(1,1,6),(6,1,3),(6,3,1),(3,6,1),(1,6,3),(3,1,6),(1,3,6),(6,6,1),(1,6,6),$$
$$(6,1,6),(6,3,3),(3,6,3),(3,3,6),(6,6,3),(3,6,6),(6,3,6),(6,6,6)\big\}.$$

Of course, realistic examples require a larger number of frequencies in order to achieve reasonable approximations of the solution. But here we aim to provide a proof of concept and we limit therefore ourselves to this frequency grid. The overall cardinality of the Gabor frame grid is $28 \cdot 120 = 3360$ and thus, the system matrix is of dimension 3360×3360. The labeling

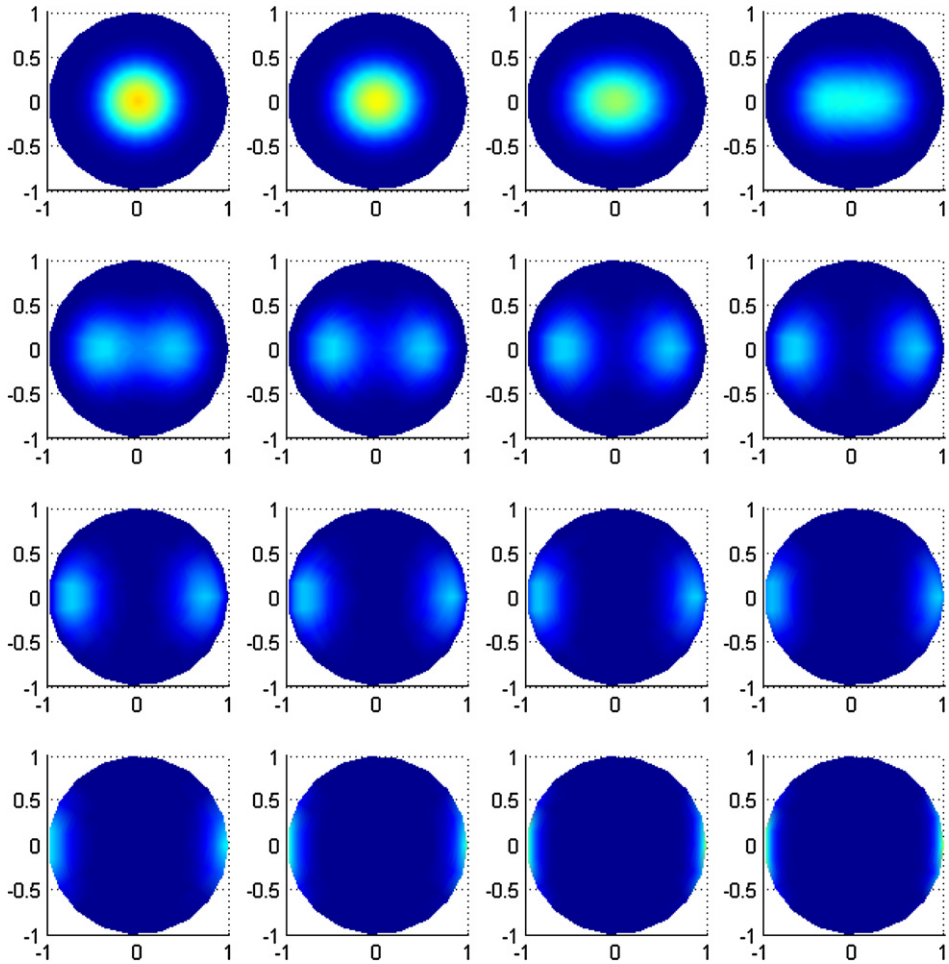

Fig. 4. Pole figures for the reconstructed crystal configuration in the noise-free scenario.

is arranged as follows: let m, $1 \leqslant m \leqslant M = 28$, denote the frequency index and j, $1 \leqslant j \leqslant J = 120$, denote the rotation index, then we set label $\gamma = \gamma(j, m) = 120(m-1) + j$. For the numerical experiment we choose a (synthetic) example of an ODF with orthorhombic crystal symmetry and triclinic symmetry for the specimen. The ODF itself is simulated by a linear combination of Gabor atoms. In particular, all coefficients in the vector c of the Gabor series expansion are set to zero except those with labels $\gamma = 1$, 46, 47, 48, 49, 50, 51, 120, they are set equal to one. The related pole figure is visualized in Fig. 2. As we have a priori knowledge about the sparsity, we set $K = 8$ (size of the ℓ_1 ball).

To simulate the measurements we derive RF^*c. In our example this corresponds to 16 equally distributed incidences rays, taking 400 measures per ray. Hereby we use a surface grid which is given by 20 Gauss quadrature nodes in each angular value. To evaluate the reconstruction capacities of the proposed algorithm (13) especially with respect to noisy data, we designed three individual experiments in which we added noise with different levels (relative data error 0%, 5% and 10%). The reconstruction results and the corresponding pole figures are illustrated in Figs. 3–8.

In the first experiment (relative error 0%, Figs. 3 and 4) we obtain a quite good approximation (Fig. 3 bottom left) of the simulated signal (Fig. 3 top left). However, the recovered magnitudes of the coefficients of c do not completely coincide with magnitudes of the simulated signal (which are one). But as the Gabor system $\{\psi_\gamma, \gamma \in \Gamma\}$ is redundant, this does not significantly effect the shape of f an therefore the magnitude of the residual discrepancy (which we wanted to minimize, Fig. 3 middle right), which is after 400 iterations 0.025867. We observe a large decay of the residual discrepancy between the 150th and 200th iteration. Afterwards the decay decreases and the step length remains nearly constant (Fig. 3 middle right, dark grey line). The residual discrepancy–sparsity plot (Fig. 3 middle left) indicates a monotone convergence (with respect to residual discrepancy) towards the preassigned sparsity level ($K = 8$).

In the second experiment we added 5% noise to the data. The arrangement of images in Figs. 5 and 6 is the same as in the first experiment. The iteration process was automatically terminated after 164 iterations (this number of iterations was necessary to achieve a residual discrepancy close to the noise level). The main observation is that we are able reconstruct a reasonable sparse approximation to the true solution (see Fig. 5 bottom left). However, the locations of the coefficients and the magnitudes are not exactly recovered, but this is feasible by the same argument as before. Fig. 5 middle right shows

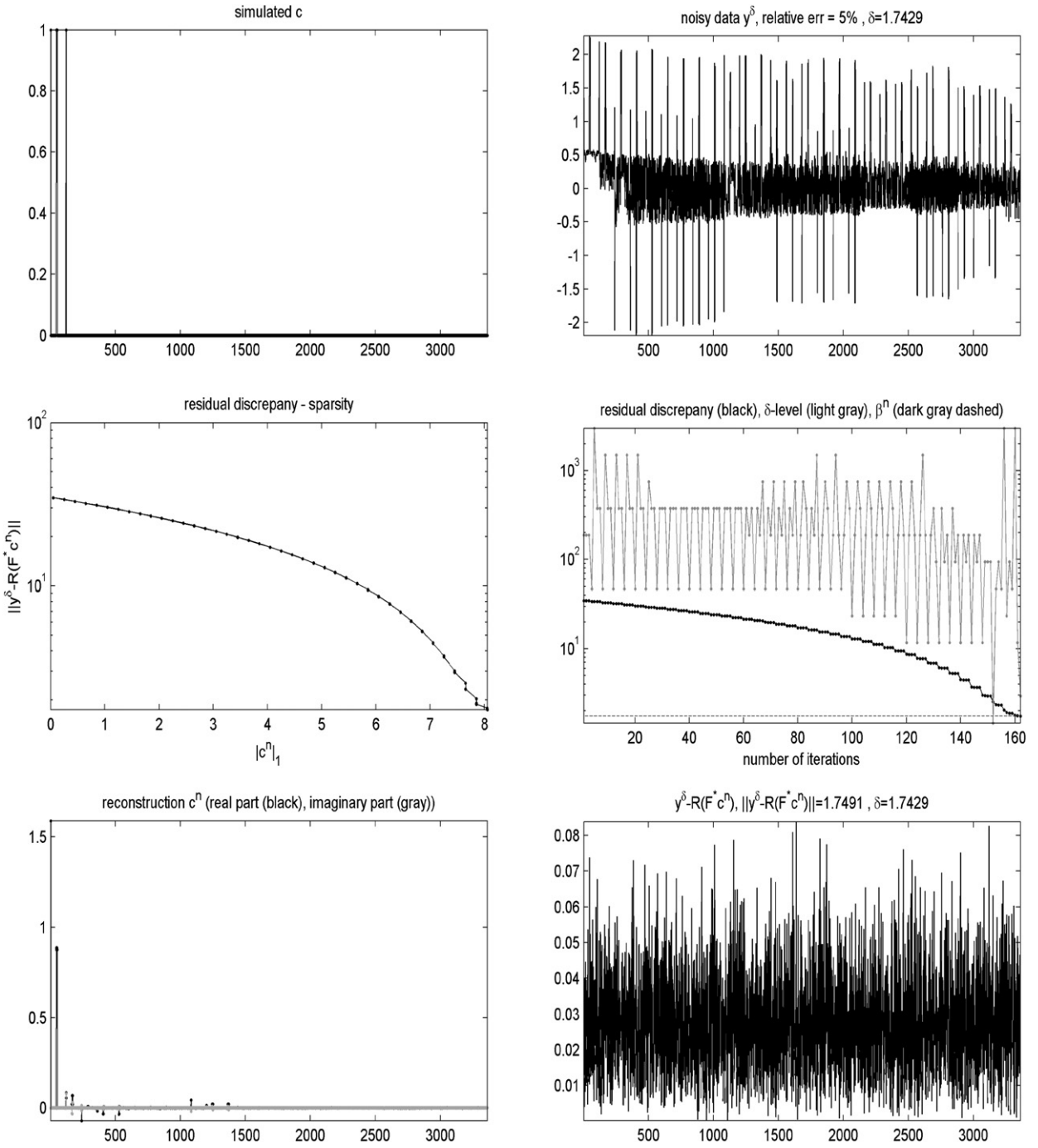

Fig. 5. Reconstruction process of iteration (13) for relative noise 5%. From top left to bottom right: simulated sequence c, simulated data y^δ, residual discrepancy (L_2 norm)–sparsity (ℓ_1 norm) plot, residual discrepancy plot including step length control β^n and noise level δ, reconstructed sequence c^n (automatically truncated after 164 iterations), residual error $y^\delta - R(F^*c^n)$.

the convergence rate and the step lengths which vary in the beginning between 70 and 500 but then tending to a small constant value as soon as the residual discrepancy has arrived the noise level. In the residual discrepancy–sparsity plot (Fig. 5 middle left) we observe that the absolute error in the beginning of the iteration process is much greater than for the noise free scenario.

The last experiment (Figs. 7 and 8) has the same design expect we added 10% noise to the data. The reconstructed coefficient vector is almost the same as in the experiment with 5% error. The only difference is the size of the residual error which is naturally of size of the noise level.

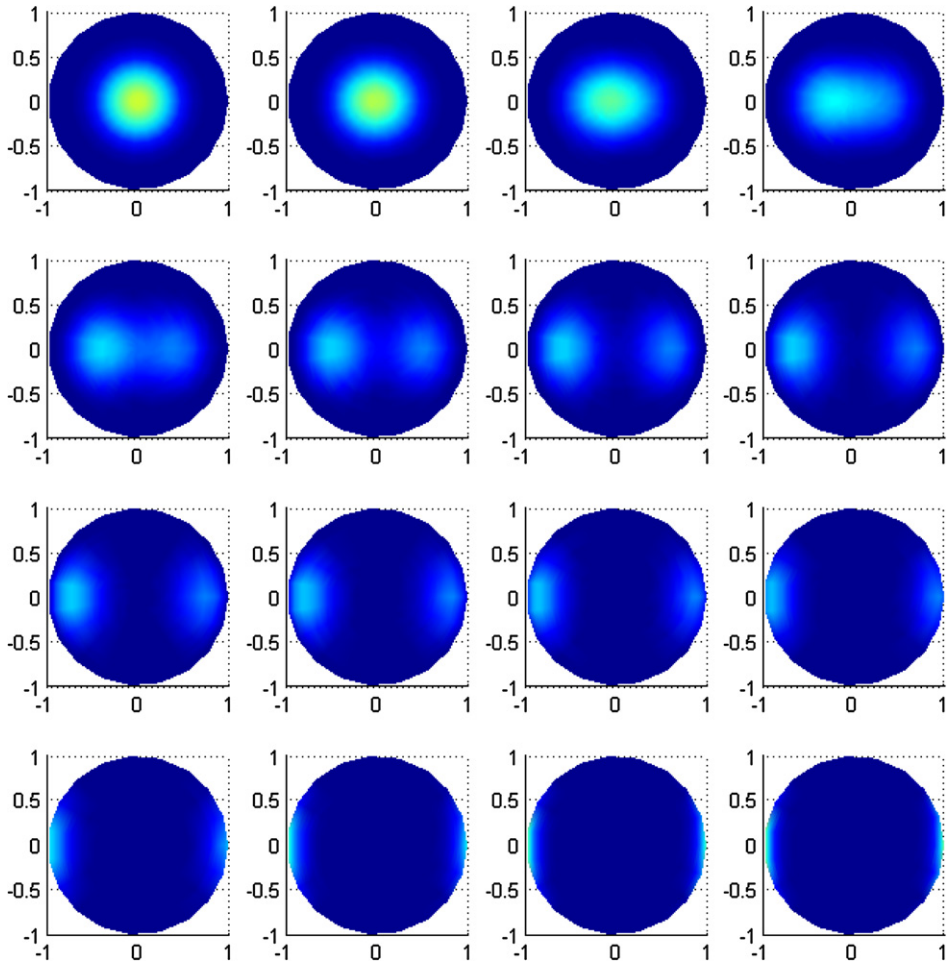

Fig. 6. Pole figures for the reconstructed crystal configuration with relative error of 5%.

Summarizing the numerical results, in each of the three experiments we were able to compute reasonable approximations to the true solution, even in the presence of noise (up to 10% relative noise). The quality of approximation depends of course naturally on the noise level. The computation of the system matrix were done on a Quad-core PC with 4 Intel Xeons E5420 @ 2.5 GHz, 8 GB RAM, Suse Linux 11, the developed code is running under Matlab 7.6.0 without any parallelization or embedded C-code. Our approach does not take any advantage of specific structure of the machine and has required an average runtime of 1703 seconds. The computation of the approximations to the true solutions were done on a Laptop (Sony VAIO, VGNZ11MN B) with Intel(R) Core(TM) 2 Duo CPU P8400 @ 2.26 GHz, 4 GB RAM, Windows XP Professional. As individual iterations might take different times (due to the determination of the optimal step length), we just provide an average overall runtime required for 200 iterations: 1153 seconds.

Acknowledgments

P. Cerejeiras, M. Ferreira and U. Kähler were supported by Acções Integradas Luso-Alemãs Acção No. A-19/08 as well as being (partially) supported by *Centro de Investigação e Desenvolvimento em Matemática e Aplicações* of University of Aveiro. G. Teschke gratefully acknowledges support by DAAD Grant D/07/13641.

Appendix A. The algebra of quaternions

A.1. Definitions

The algebra of quaternions $\mathbb{H}$ is a four-dimensional real associative division algebra with unit 1 spanned by the elements $\{e_1, e_2, e_3\}$ endowed with the relations

$$e_1^2 = e_2^2 = e_3^2 = -1,$$

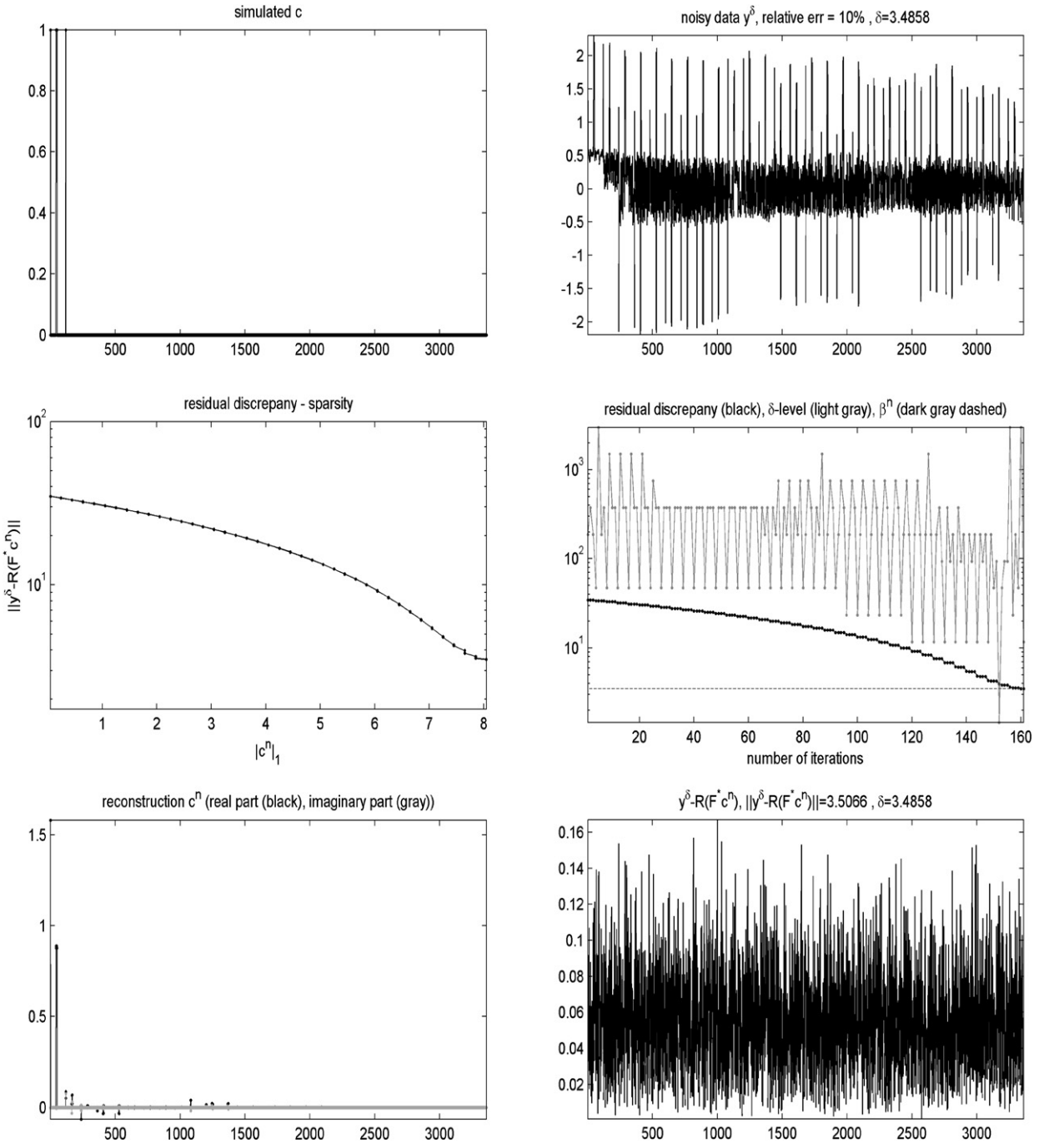

Fig. 7. Reconstruction process of iteration (13) for the noise-free scenario. From top left to bottom right: simulated sequence c, simulated data y^δ, residual discrepancy (L_2 norm)–sparsity (ℓ_1 norm) plot, residual discrepancy plot including step length control β^n and noise level δ, reconstructed sequence c^n (automatically truncated after 161 iterations), residual error $y^\delta - R(F^* c^n)$.

$$e_1 e_2 = -e_2 e_1 = e_3, \qquad e_2 e_3 = -e_3 e_2 = e_1, \qquad e_1 e_3 = -e_3 e_1 = e_2.$$

This algebra is a non-commutative field. The real and imaginary parts of a given quaternion

$$q = x_0 1 + x_1 e_1 + x_2 e_2 + x_3 e_3$$

are defined as $Re(q) = q_0 := x_0$, and $Im(q) = \vec{q} := x_1 e_1 + x_2 e_2 + x_3 e_3$. Therefore, in contrast to complex numbers, $\vec{q}$ is not a real number. We have then natural embeddings of the real numbers and of $\mathbb{R}^3$ into quaternions given by

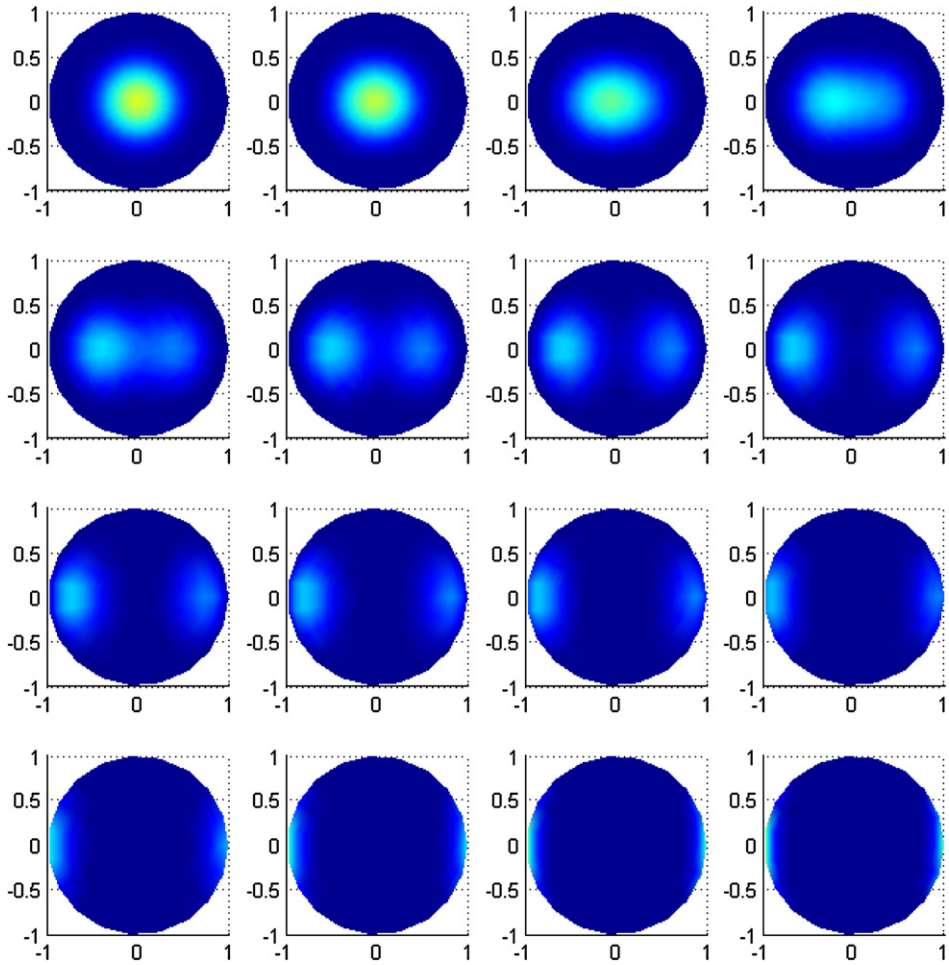

Fig. 8. Pole figures for the reconstructed crystal configuration with relative error of 10%.

$$x_0 \in \mathbb{R} \to x_0 1 \in \mathbb{H} \quad \text{and} \quad (x_1, x_2, x_3) \in \mathbb{R}^3 \to x_1 e_1 + x_2 e_2 + x_3 e_3 \in \mathbb{H}.$$

Moreover, we have the identifications $\mathbb{H} \equiv \mathbb{R}^4$, $Im\,\mathbb{H} \equiv \mathbb{R}^3$, $Re\,\mathbb{H} \equiv \mathbb{R}$, where $Im\,\mathbb{H}$ is the three-dimensional space of imaginary quaternions, and $\mathbb{H} = \mathbb{R} \oplus \mathbb{R}^3$.

There is a suitable conjugation on $\mathbb{H}$, given by

$$q = x_0 + \vec{q} \to \bar{q} = x_0 - \vec{q}$$

and satisfying to the involution property $\overline{qp} = \bar{p}\bar{q}$. The Euclidean scalar product is defined on $\mathbb{H} = \mathbb{R}^4$ by $\langle q, p\rangle = Re(q\bar{p}) = \frac{1}{2}(q\bar{p} + p\bar{q})$ and the corresponding norm $\|q\|^2 = \langle q, q\rangle$ verifies $\|qp\| = \|q\|\|p\|$. The quaternionic multiplication can be expressed in terms of the usual scalar and vector product on $Im\,\mathbb{H} \equiv \mathbb{R}^3$ by

$$qp = (q_0 + \vec{q})(p_0 + \vec{p}) = q_0 p_0 - \vec{q} \cdot \vec{p} + q_0 \vec{p} + p_0 \vec{q} + \vec{q} \times \vec{p}.$$

A.2. Rotations in $\mathbb{R}^3$ and $\mathbb{R}^4$

The set of unitary quaternions $S^3 = \{q \in \mathbb{H},\ \|q\| = 1\}$ is a group under multiplication. It can be interpreted also as a group of linear maps $p \in \mathbb{H} \to qp$ which preserves the ($\mathbb{H}$-valued) hermitian product $p|q = \bar{p}q$ and it is usually called the symplectic group $Sp(1)$. The action of $Sp(1)$ on $\mathbb{H}$ given by $\hat{\rho}(q) : \mathbb{H} \to \mathbb{H}$, $\hat{\rho}(q)p = qp\bar{q}$, $q \in Sp(1)$ preserves the Euclidean scalar product on $\mathbb{R}^4$, it stabilizes $\mathbb{R} \subset \mathbb{H}$ and its orthogonal complement $Im\,\mathbb{H}$. Also, we define the automorphic groups $SO(3)$ and $SO(4)$ as

$$SO(3) = \left\{T \in Aut(\mathbb{H}) \colon\ (T\vec{q}) \cdot (T\vec{p}) = \vec{q} \cdot \vec{p},\ \vec{q}, \vec{p} \in \mathbb{R}^3 \equiv Im\,\mathbb{H}\right\},$$

and

$$SO(4) = \left\{ Q \in Aut(\mathbb{H}):\ \langle Qq, Qp\rangle = \langle q, p\rangle,\ q, p \in \mathbb{H} \right\}.$$

The restriction of the action of the group $Sp(1)$ on $\mathbb{R}^3 = Im\mathbb{H}$ is a representation of $Sp(1)$ by rotations and it induces a homomorphism $\hat{\rho} : Sp(1) \to SO(3)$ which can be shown to be the universal covering of the group $SO(3) \simeq Sp(1)/\mathbb{Z}_2$. Hence $Sp(1)$ is also isomorphic to $Spin(3)$.

Finally, the map $\rho:\ Sp(1) \times Sp(1) \to SO(4)$, $(u, v) \to \rho(u, v)(q) = uq\bar{v}$ preserves the Euclidean norm in $\mathbb{R}^4$, that is,

$$\|uq\bar{v}\|^2 = Re(uq\bar{v}\overline{uq\bar{v}}) = Re(uq\bar{v}v\bar{q}\bar{u}) = Re(q\bar{q}) = \|q\|^2.$$

Therefore, we have a homomorphism of $Sp(1) \times Sp(1)$. Moreover, it can be shown that ρ defines a two-fold covering of the special orthogonal group $SO(4)$ and so, we have $Spin(4) \equiv Sp(1) \times Sp(1)$.

References

[1] A. Averbuch, E. Braverman, R. Coifman, M. Israeli, A. Sidi, Efficient computation of oscillatory integrals via adaptive multiscale local Fourier bases, Appl. Comput. Harmon. Anal. 9 (1) (2000) 19–53.
[2] A. Averbuch, E. Braverman, R. Coifman, M. Israeli, On efficient computation of multidimensional oscillatory integrals with local Fourier bases, Nonlinear Anal. Ser. A: Theory and Methods 47 (5) (2001) 3491–3502.
[3] S. Bernstein, H. Schaeben, A one-dimensional Radon transform on SO(3) and its application to texture goniometry, Math. Methods Appl. Sci. 28 (2005) 126989.
[4] K.G. v.d. Boogaart, R. Hielscher, J. Prestin, H. Schaeben, Kernel-based methods for inversion of the radon transform on SO(3) and their applications to texture analysis, J. Comput. Appl. Math. 199 (2007) 122–140.
[5] H.J. Bunge, Texture Analysis in Material Science, Butterworths, London, 1982.
[6] P. Cerejeiras, H. Schaeben, F. Sommen, The spherical X-ray transform, Math. Methods Appl. Sci. 25 (2002) 1493507.
[7] S. Dahlke, G. Steidl, G. Teschke, Frames and coorbit theory on homogeneous spaces with a special guidance on the sphere, in: Special Issue: Analysis on the Sphere, J. Fourier Anal. Appl. 13 (4) (2007) 387–403.
[8] S. Dahlke, G. Steidl, G. Teschke, Weighted coorbit spaces and Banach frames on homogeneous spaces, J. Fourier Anal. Appl. 10 (5) (2004) 507–539.
[9] I. Daubechies, M. Fornasier, I. Loris, Accelerated projected gradient methods for linear inverse problems with sparsity constraints, J. Fourier Anal. Appl. 14 (5–6) (2008) 764–792.
[10] I. Daubechies, M. Defrise, C. DeMol, An iterative thresholding algorithm for linear inverse problems with a sparsity constraint, Comm. Pure Appl. Math. 57 (2004) 1413–1541.
[11] I. Daubechies, G. Teschke, Variational image restoration by means of wavelets: simultaneous decomposition, deblurring and denoising, Appl. Comput. Harmon. Anal. 19 (1) (2005) 1–16.
[12] I. Daubechies, G. Teschke, L. Vese, Iteratively solving linear inverse problems with general convex constraints, Inverse Probl. Imaging 1 (1) (2007) 29–46.
[13] I. Daubechies, G. Teschke, L. Vese, On some iterative concepts for image restoration, Adv. Imaging Electron Phys. 150 (2008) 1–51.
[14] R. Delanghe, F. Sommen, V. Souček, Clifford Analysis and Spinor-Valued Functions: A Function Theory for the Dirac Operator, Math. Appl., vol. 53, Kluwer Acad. Publ., Dordrecht, 1992.
[15] R. Hielscher, The Radon transform on the rotation group inversion and application to texture analysis, Dissertation, Department of Geosciences, University of Technology Freiberg, 2007, https://fridolin.tufreiberg.de/archiv/html/MathematikHielscherRalf361401.html.
[16] R. Hielscher, D. Potts, J. Prestin, H. Schaeben, M. Schmalz, The Radon transform on $SO(3)$: a Fourier slice theorem and numerical inversion, Inverse Problems 24 (2008), doi:10.1088/0266-5611/24/2/025011.
[17] U.F. Kocks, C.N. Tomé, H.R. Wenk, H. Mecking, Texture and Anisotropy, Cambridge University Press, Cambridge, 1998.
[18] S. Matthies, G. Vinel, K. Helmig, Standard Distributions in Texture Analysis, vol. 1, Akademie-Verlag, Berlin, 1987.
[19] G. Matviyenko, Optimized local trigonometric bases, Appl. Comput. Harmon. Anal. 3 (1996) 301–323.
[20] L. Meister, H. Schaeben, A concise quaternion geometry of rotations, MMAS 28 (2004) 101126.
[21] G. Nawratil, H. Pottmann, Subdivision schemes for the fair discretization of the spherical motion group, Technical Report, Vienna University of Technology, June 2007.
[22] D.I. Nikolayev, H. Schaeben, Characteristics of the ultra-hyperbolic differential equation governing pole density functions, Inverse Problems 15 (1999) 160319.
[23] R. Ramlau, G. Teschke, M. Zhariy, A compressive Landweber iteration for solving ill-posed inverse problems, Inverse Problems 24 (6) (2008) 065013.
[24] V. Randle, O. Engler, Introduction to Texture Analysis Macrotexture: Microtexture and Orientation Mapping, Gordon and Breach, London, 2000.
[25] H. Schaeben, K.G.v.d. Boogaart, Spherical harmonics in texture analysis, Tectonophysics 370 (2003) 253–268.
[26] H. Schaeben, R. Hielscher, J. Fundenberger, D. Potts, J. Prestin, Orientation density function-controlled pole probability density function measurements: automated adaptive control of texture goniometers, J. Appl. Crystallogr. 40 (3) (2007) 570–579.
[27] G. Teschke, Multi-frame representations in linear inverse problems with mixed multi-constraints, Appl. Comput. Harmon. Anal. 22 (2007) 43–60.
[28] G. Teschke, C. Borries, Accelerated projected steepest descent method for nonlinear inverse problems with sparsity constraints, Inverse Problems 26 (2010) 025007.
[29] B. Torrésani, Phase space decompositions: local Fourier analysis on spheres, preprint CPT-93/P.2878, Marseille, 1993; Signal Process. 43 (1995) 341–346.